Hierarchy of Visual Processing

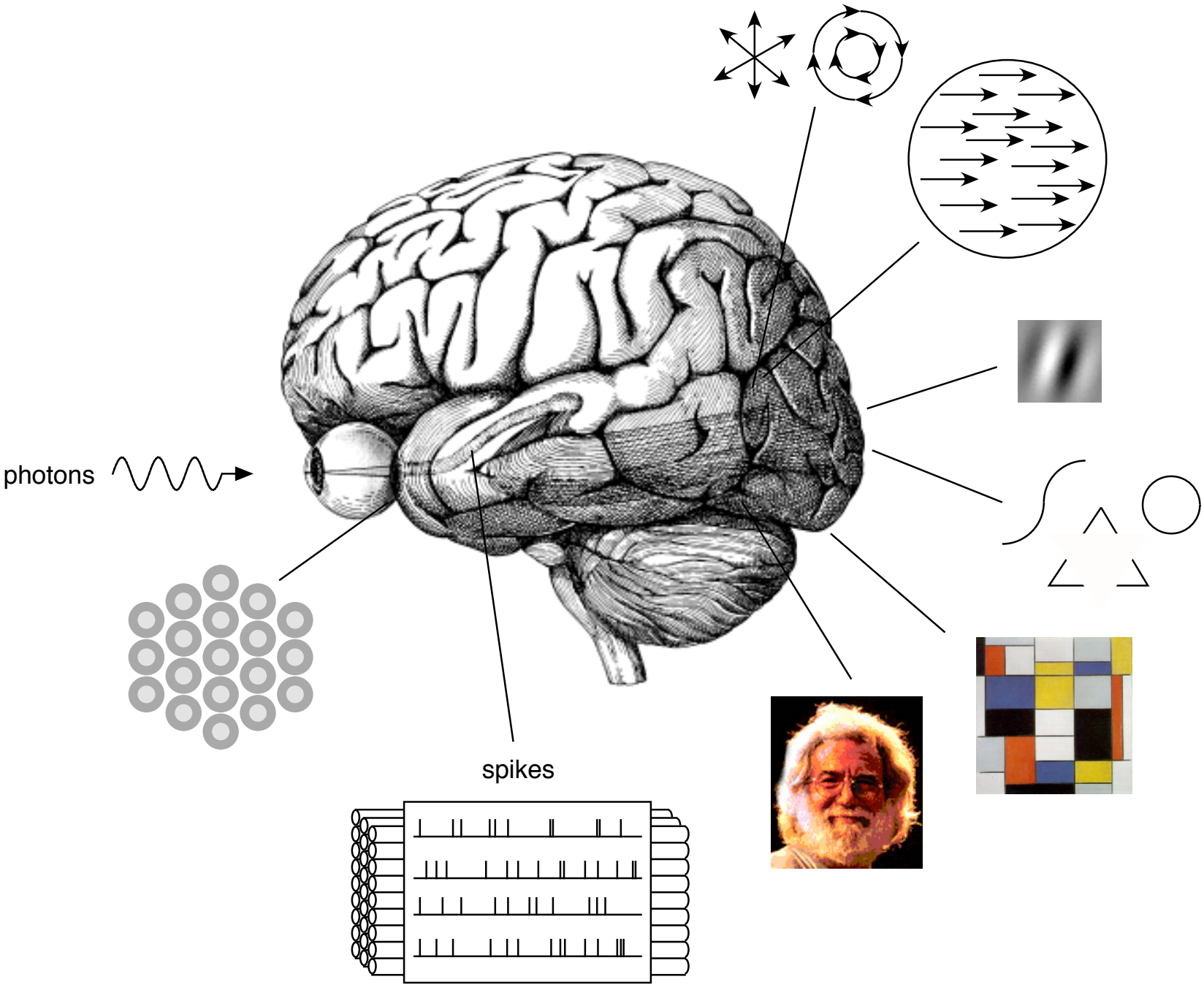

Projections of the retina

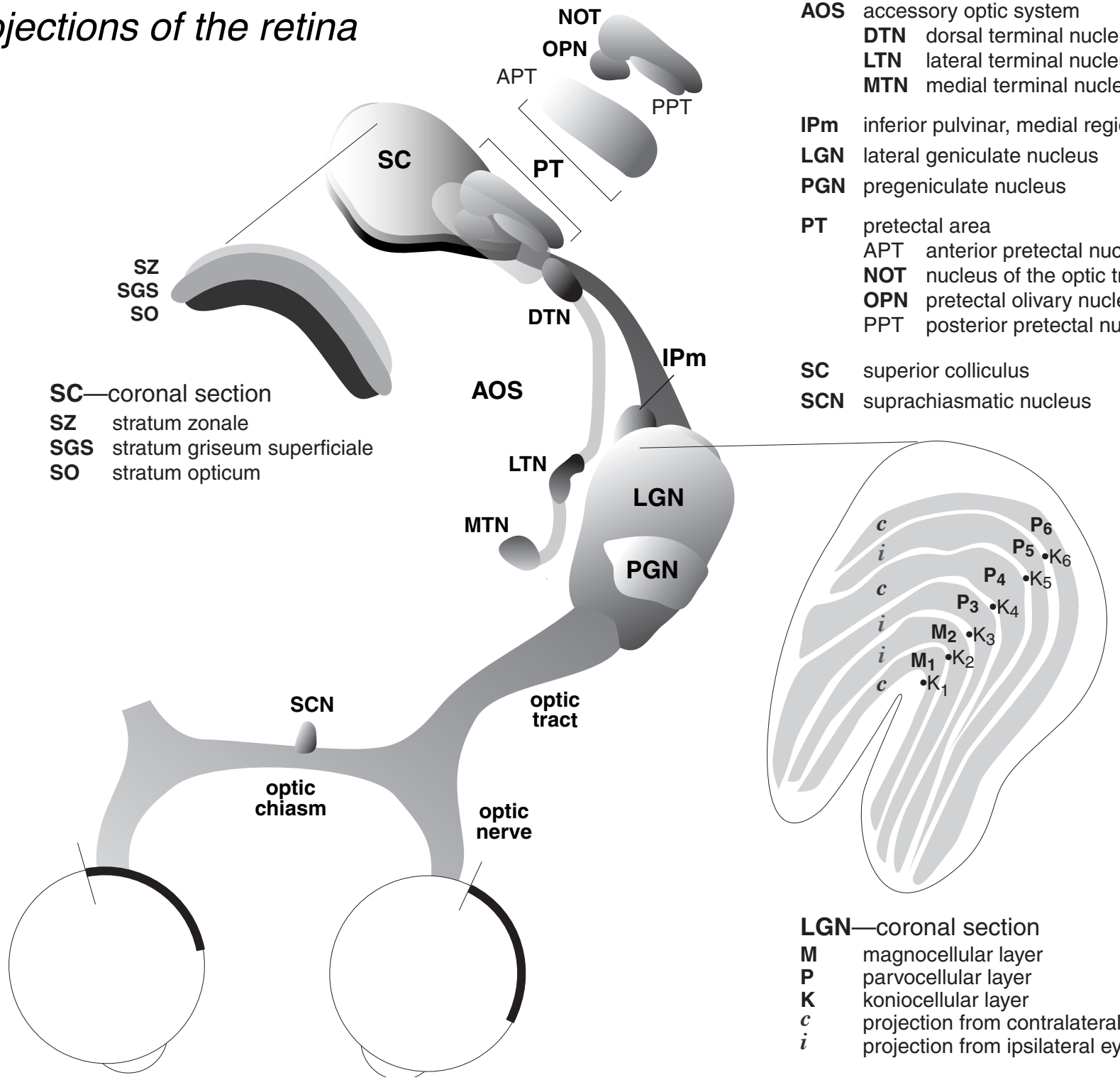

AOS accessory optic system
- **DTN** dorsal terminal nucleus
- **LTN** lateral terminal nucleus
- **MTN** medial terminal nucleus

IPm inferior pulvinar, medial region

LGN lateral geniculate nucleus

PGN pregeniculate nucleus

PT pretectal area
- APT anterior pretectal nucleus
- **NOT** nucleus of the optic tract
- **OPN** pretectal olivary nucleus
- PPT posterior pretectal nucleus

SC superior colliculus

SCN suprachiasmatic nucleus

SC—coronal section
- **SZ** stratum zonale
- **SGS** stratum griseum superficiale
- **SO** stratum opticum

LGN—coronal section
- **M** magnocellular layer
- **P** parvocellular layer
- **K** koniocellular layer
- *c* projection from contralateral eye
- *i* projection from ipsilateral eye

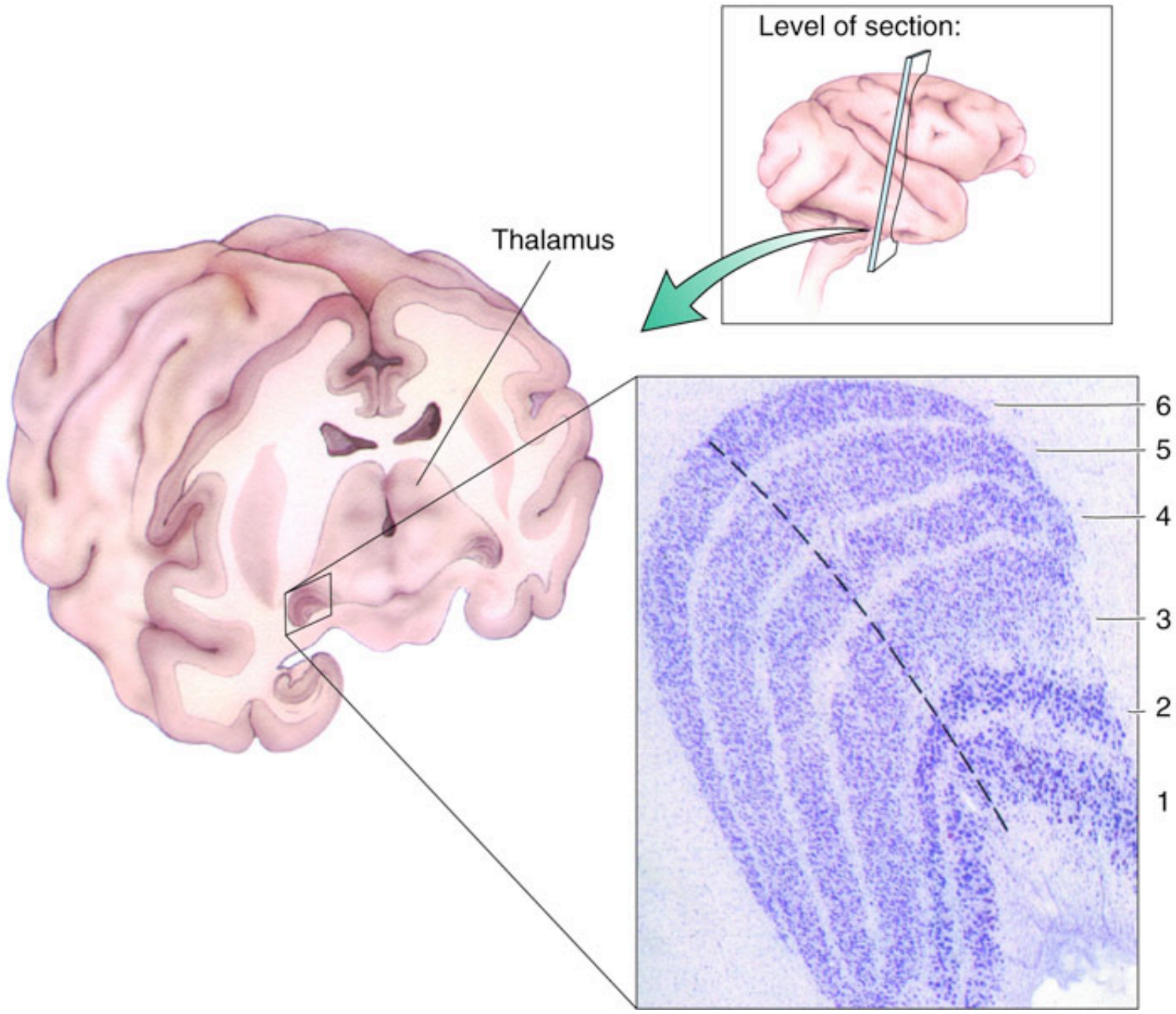
Level of section:
Thalamus
6
5
4
3
2
1

Monkey LGN

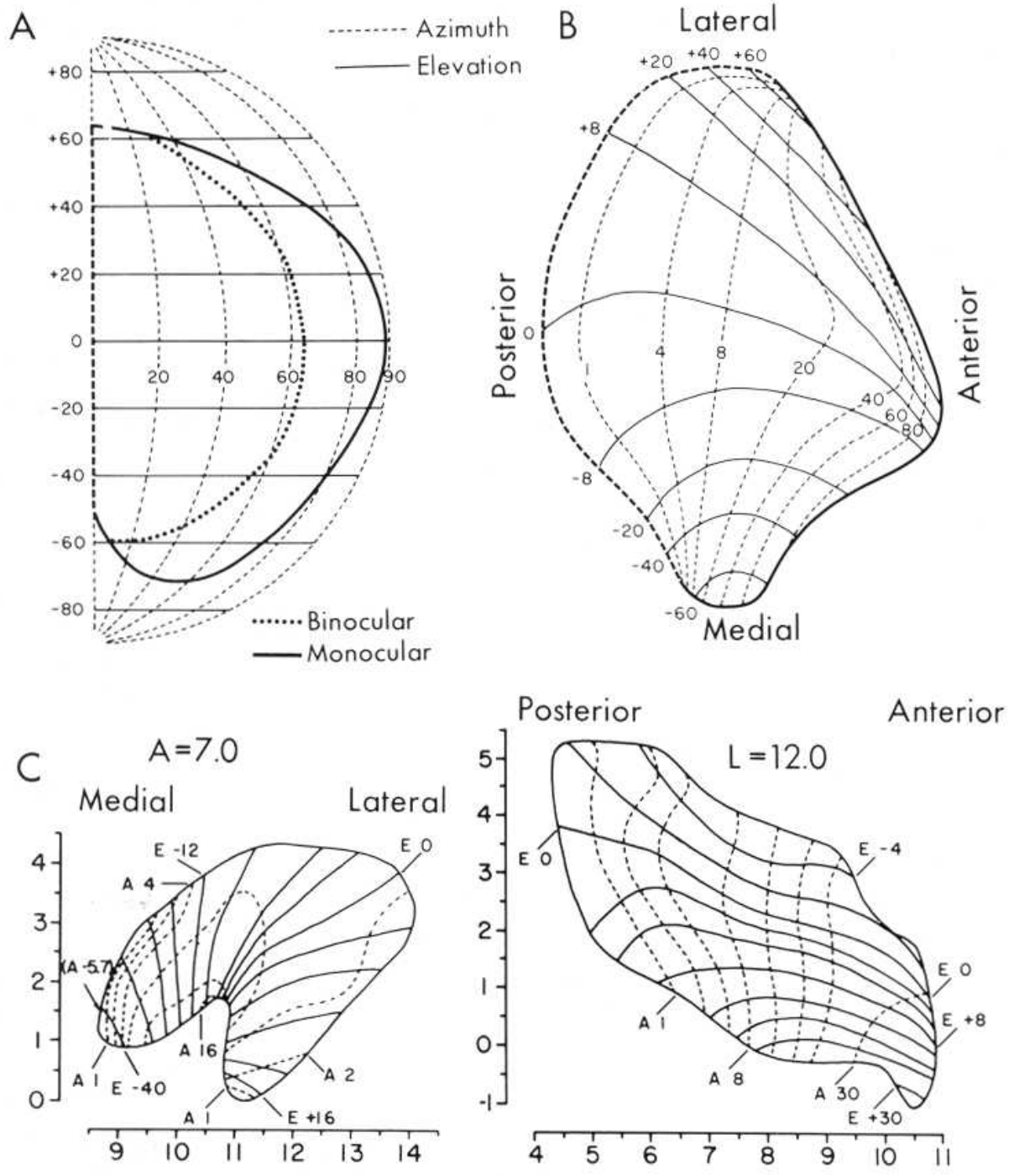
A
Azimuth
Elevation
+80
+60
+40
+20
0
-20
-40
-60
-80
20
40
60
80
90
Binocular
Monocular
B
Lateral
+20
+40
+60
+8
0
-8
-20
-40
-60
4
8
20
40
60
80
Posterior
Anterior
Medial
C
A=7.0
Medial
Lateral
E -12
E 0
A 4
(A -5.7)
A 16
A 2
A 1
E -40
A 1
E +16
9
10
11
12
13
14
Posterior
Anterior
L=12.0
E 0
E -4
E 0
E +8
A 1
A 8
A 30
E +30
4
5
6
7
8
9
10
11

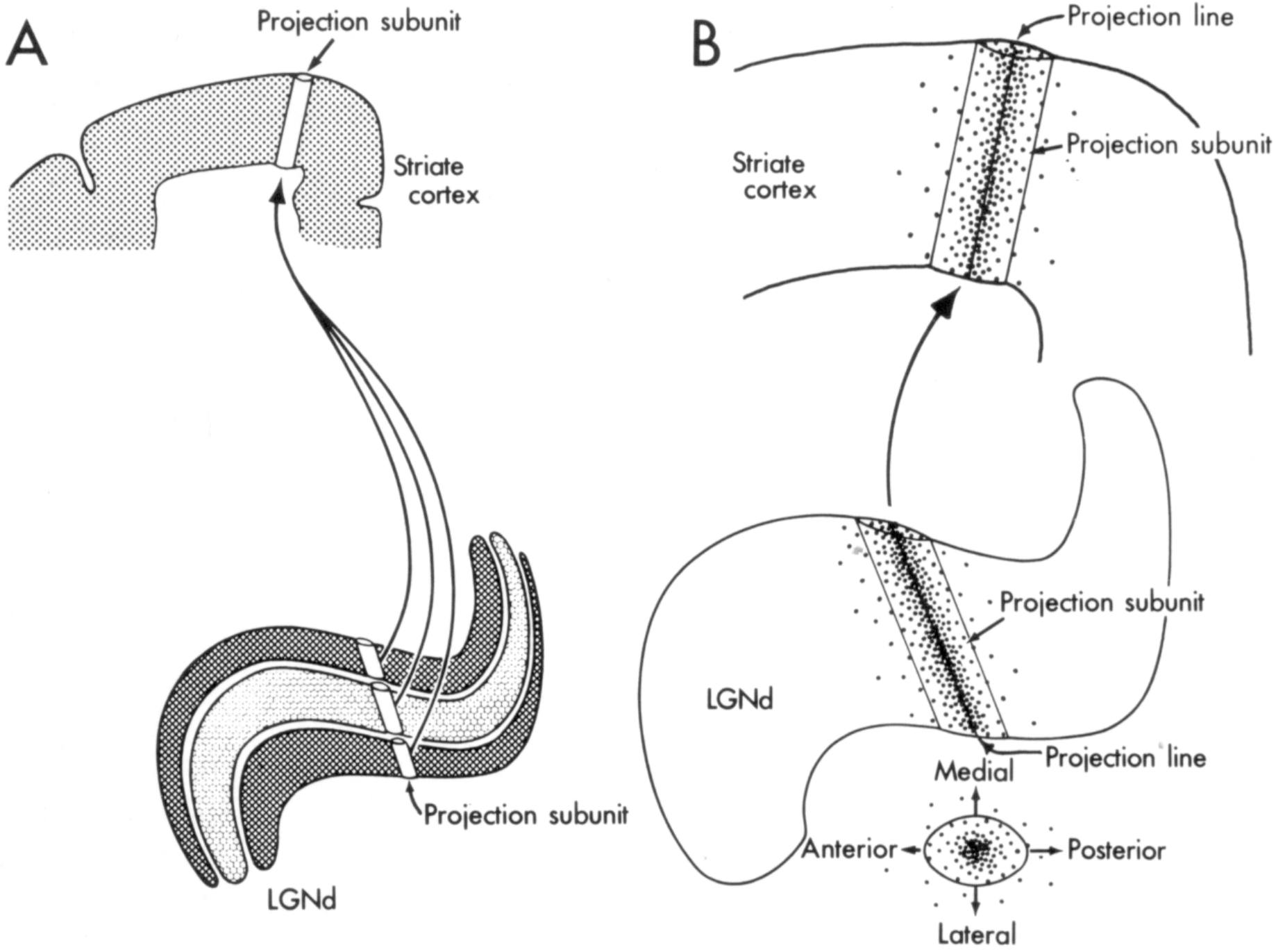
A
Projection subunit
Striate cortex
Projection subunit
LGNd
B
Projection line
Striate cortex
Projection subunit
Projection subunit
LGNd
Projection line
Medial
Anterior
Posterior
Lateral

Cat LGN

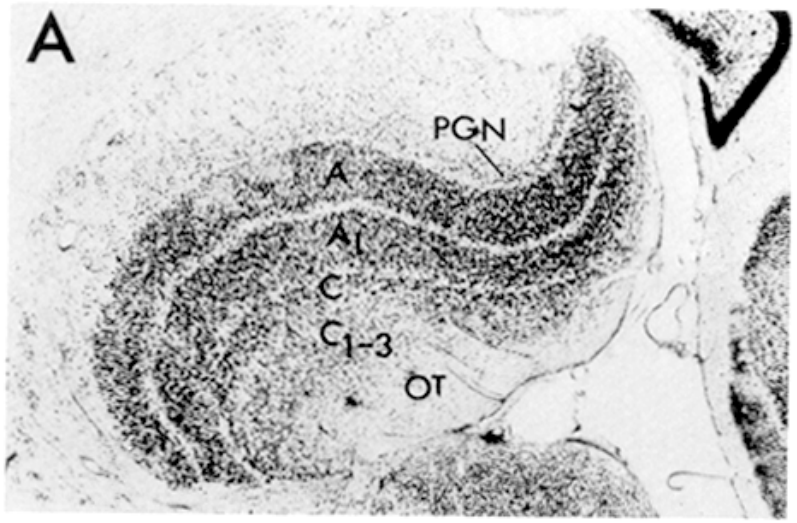
A
PGN
A
A1
C
C1-3
OT

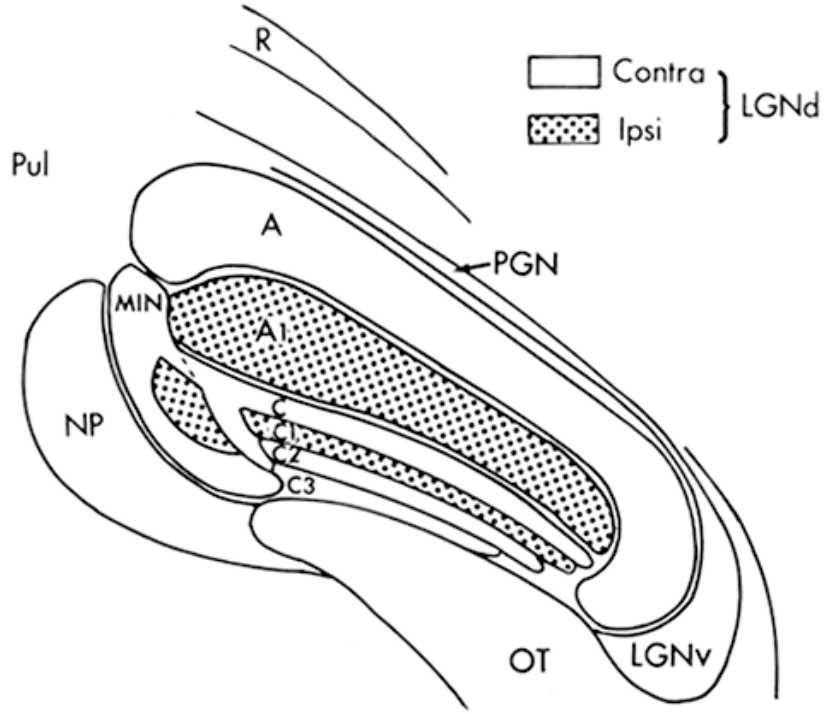
B
R
Contra
Ipsi
LGNd
Pul
A
PGN
MIN
A1
NP
C1
C2
C3
OT
LGNv

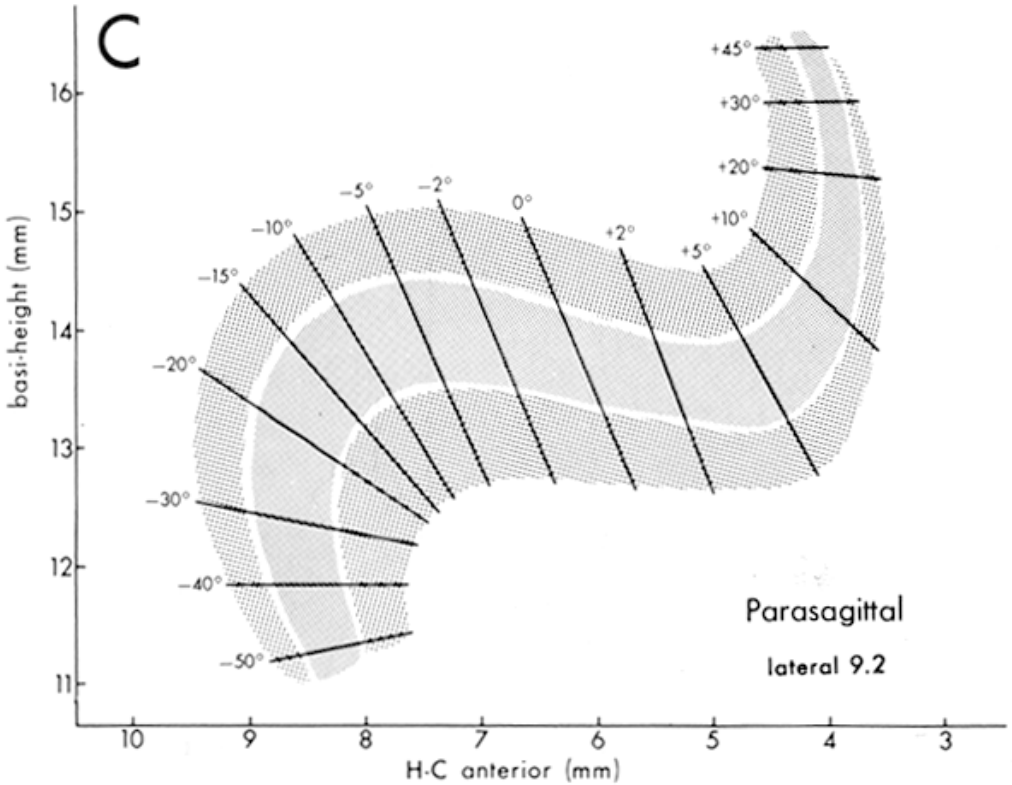
C
basi-height (mm)
H-C anterior (mm)
+45°
+30°
+20°
+10°
+5°
+2°
0°
-2°
-5°
-10°
-15°
-20°
-30°
-40°
-50°
Parasagittal
lateral 9.2

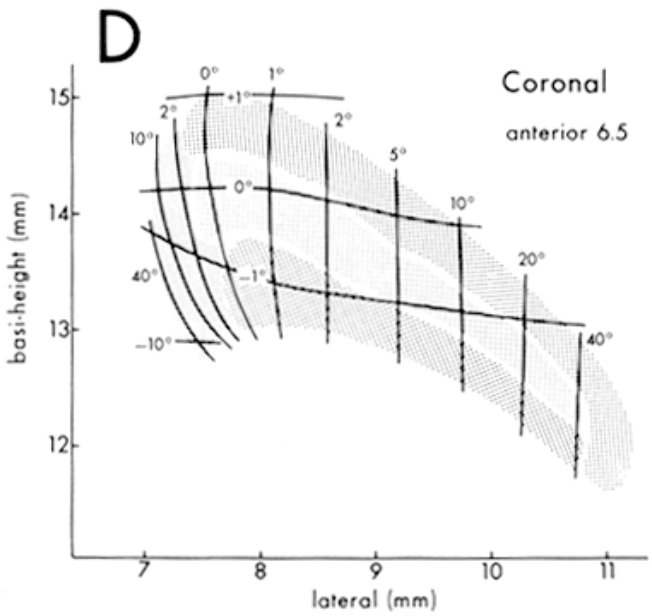
D
Coronal
anterior 6.5
basi-height (mm)
lateral (mm)
0°
1°
2°
5°
10°
20°
40°
-1°
-10°

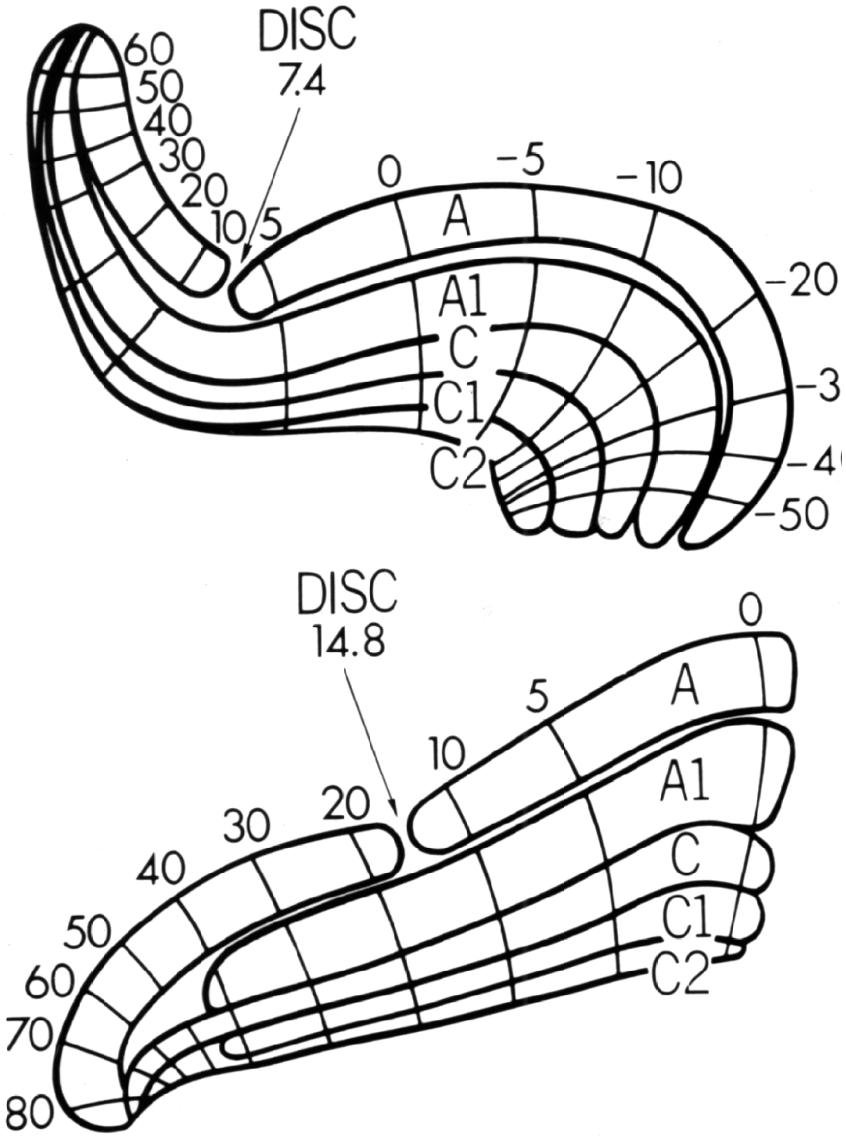

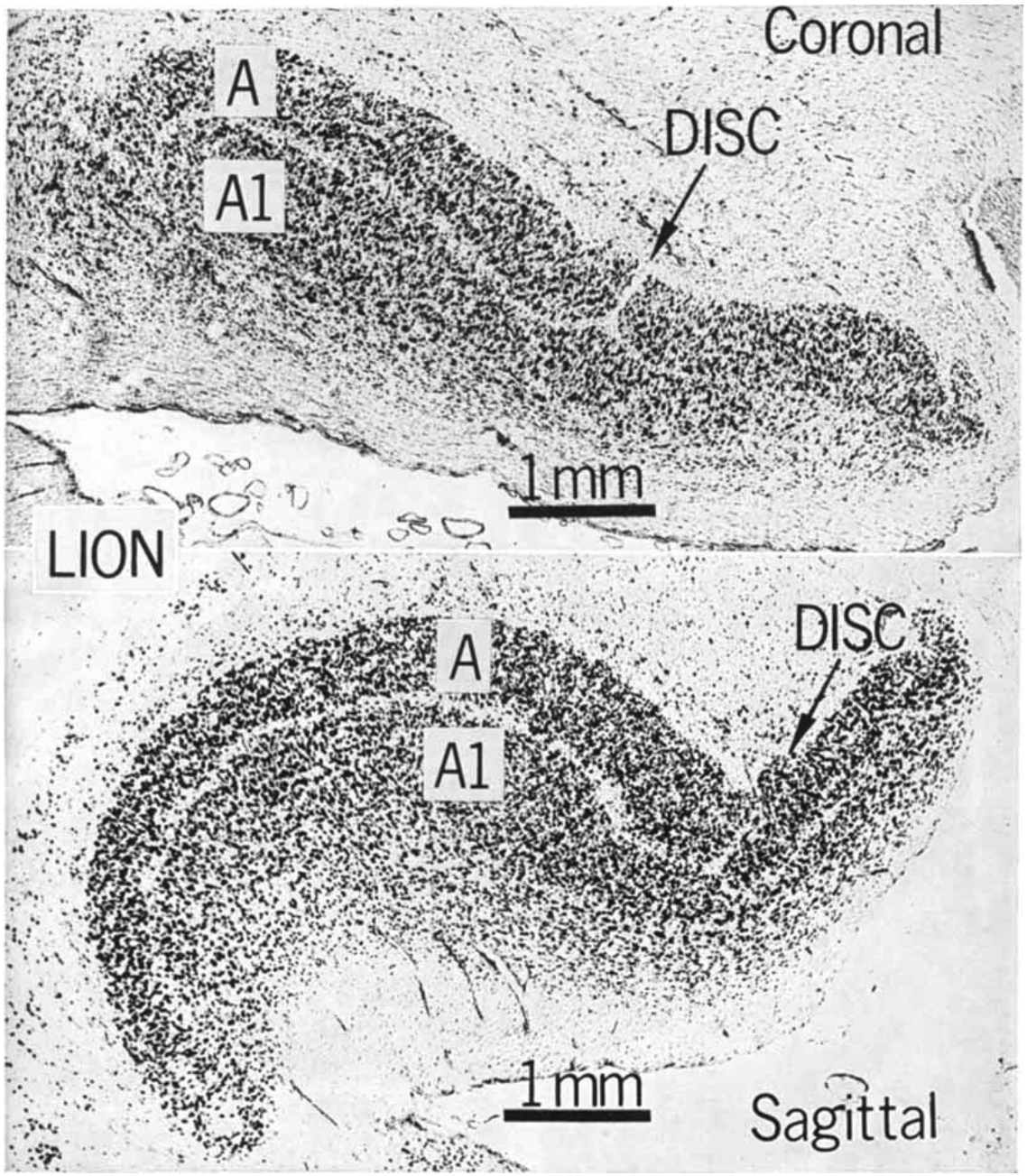

Fig. 2 The lateral geniculate nucleus of a lion in coronal and sagittal sections. The cellular discontinuity in layer A (DISC) is shown. Medial is to the left in the upper figure and rostral is to the left in the lower figure. Thionin stain.

Responses in the retina and the LGN are more or less the same

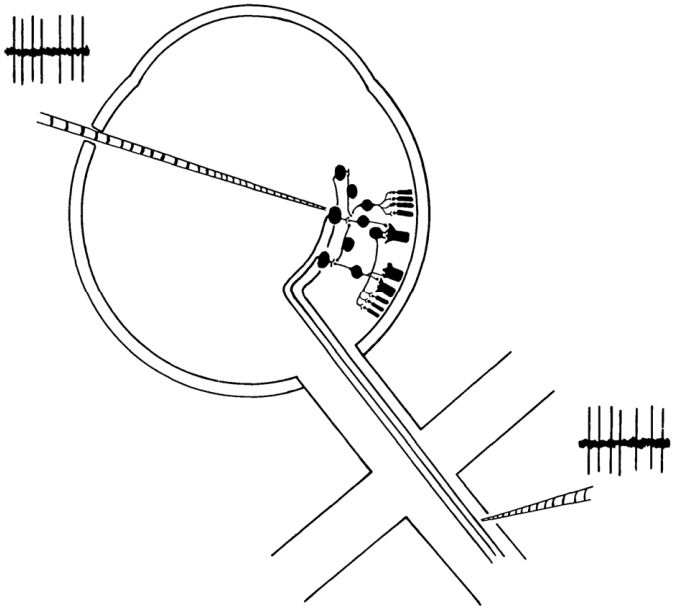

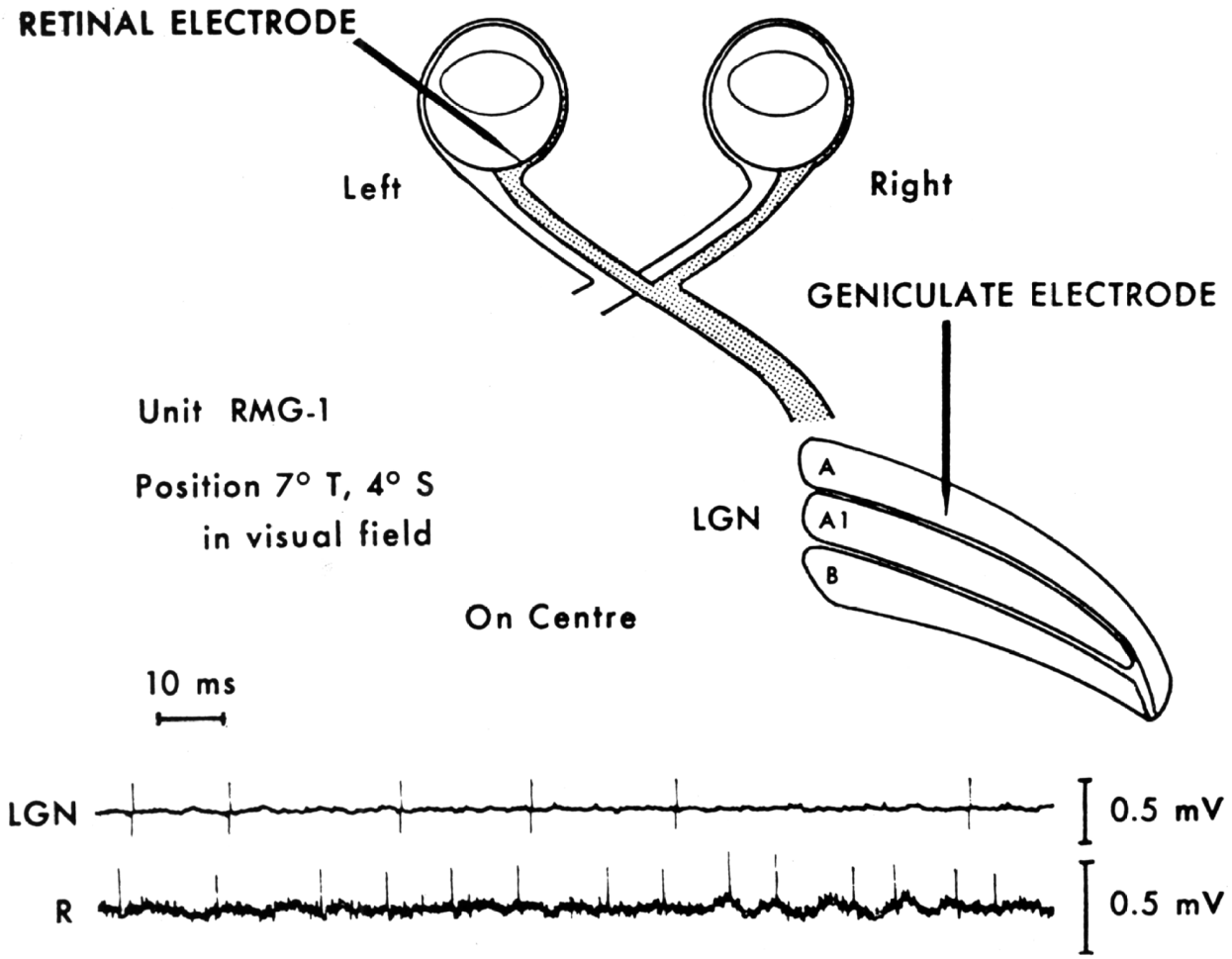

Cleland, Dubin & Levick (1971)

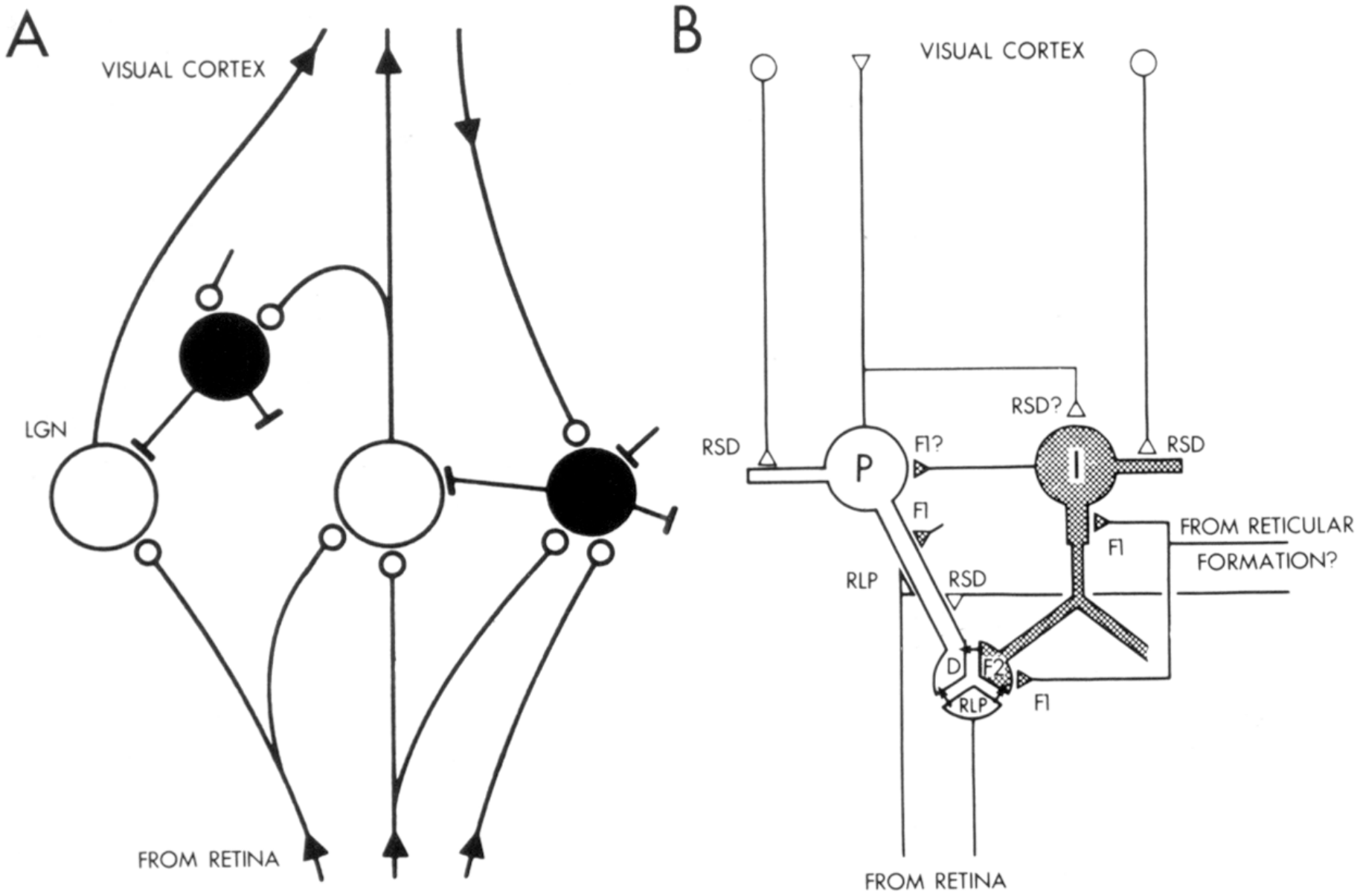
A
VISUAL CORTEX
LGN
FROM RETINA
B
VISUAL CORTEX
RSD?
RSD
F1?
P
I
RSD
F1
FROM RETICULAR
FORMATION?
F1
RLP
RSD
D
F2
RLP
F1
FROM RETINA

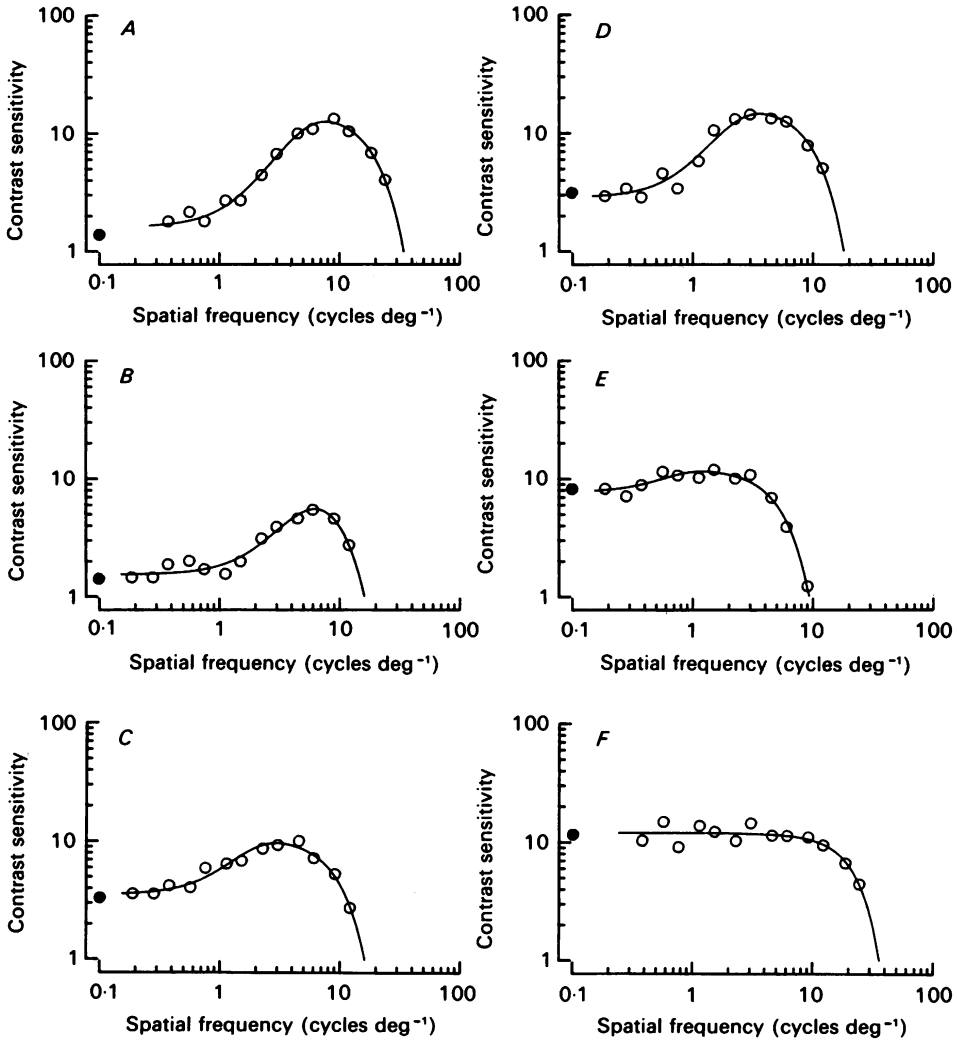

Fig. 3. Spatial contrast sensitivity of parvocellular units to sinusoidal gratings moving at 5·2 Hz. Filled circles on the ordinates mark the sensitivity to modulation of a spatially uniform field. *A*, *C* and *E*, type I units; *B* and *D*, type III units; *F*, type II unit driven by R and G cones.

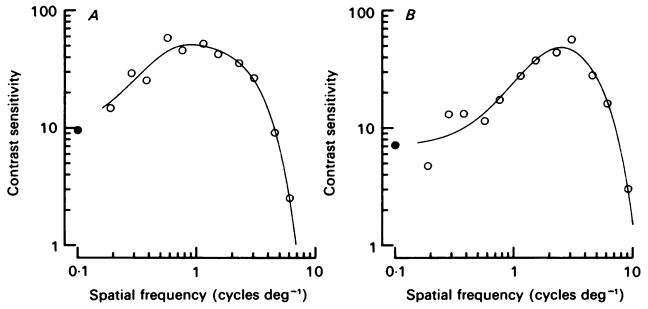

Fig. 10. Spatial contrast sensitivity functions obtained from magnocellular units, using gratings moving at 5·2 Hz. Filled circles on the ordinates mark sensitivities to modulation of a spatially uniform field. *A*, unit that showed linear spatial summation; *B*, unit that showed substantially non-linear spatial summation.

Contrast responses of M and P cells in macaque LGN

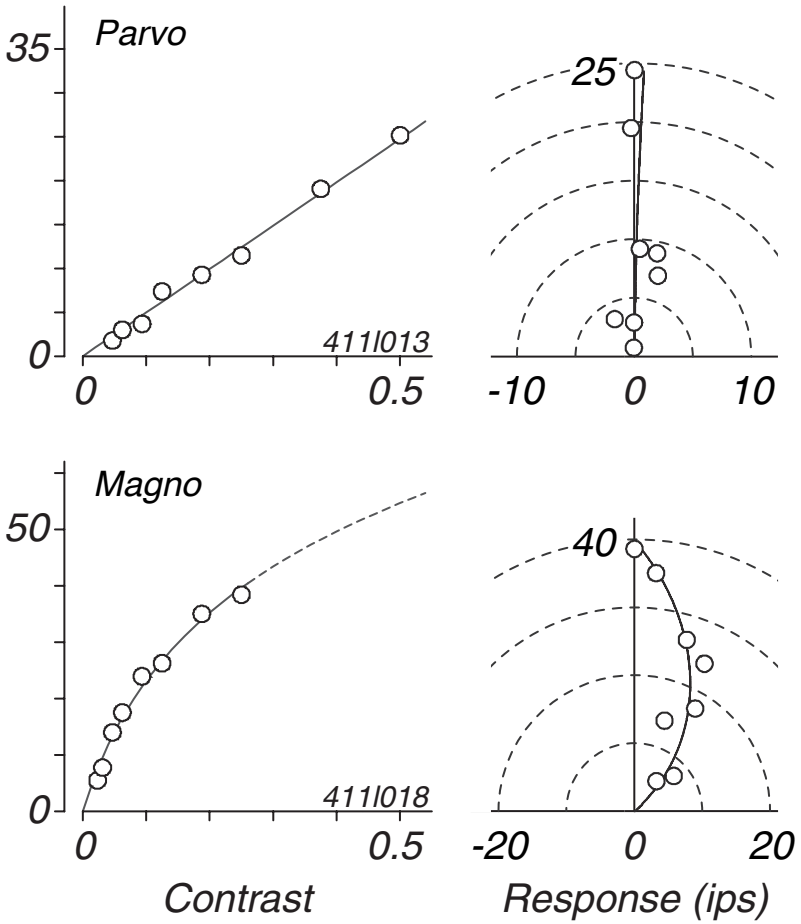

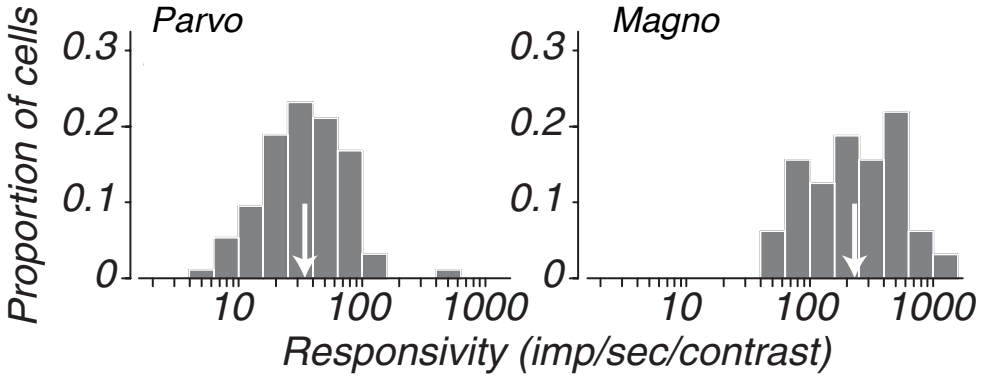

Movshon et al, 2005

K cells in marmoset LGN

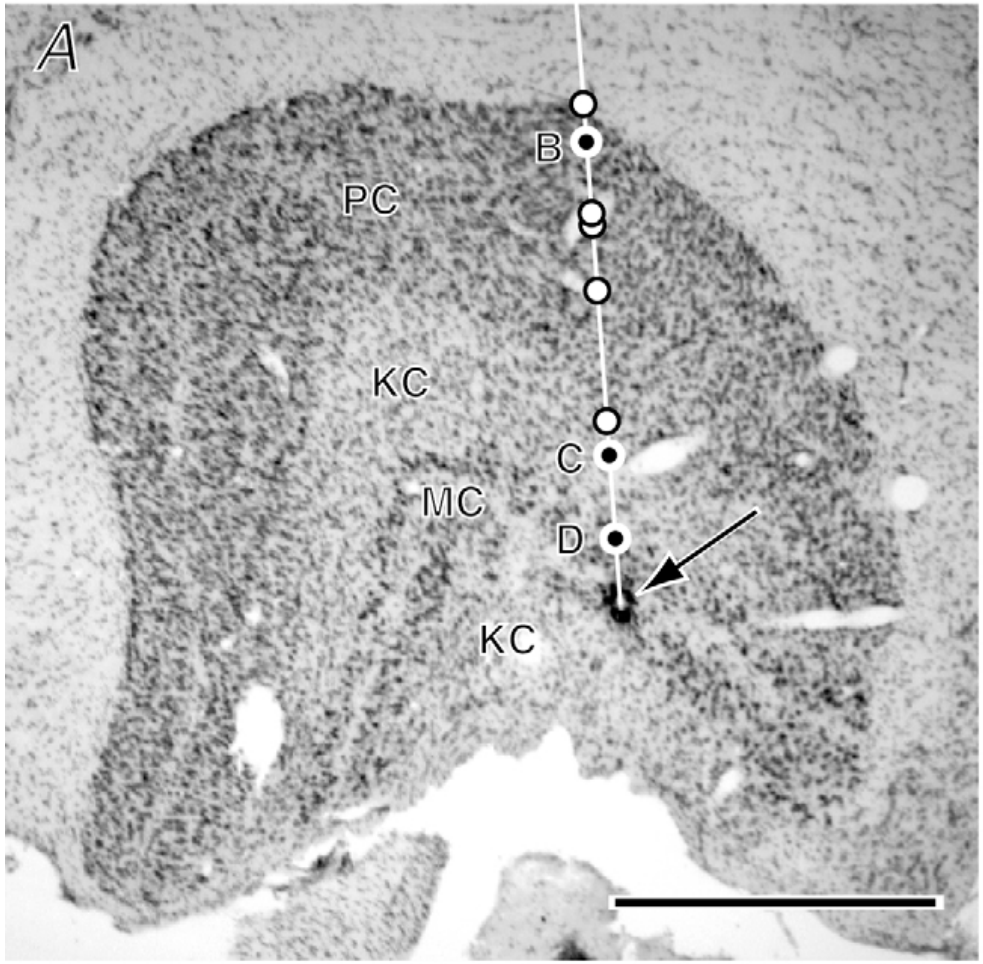

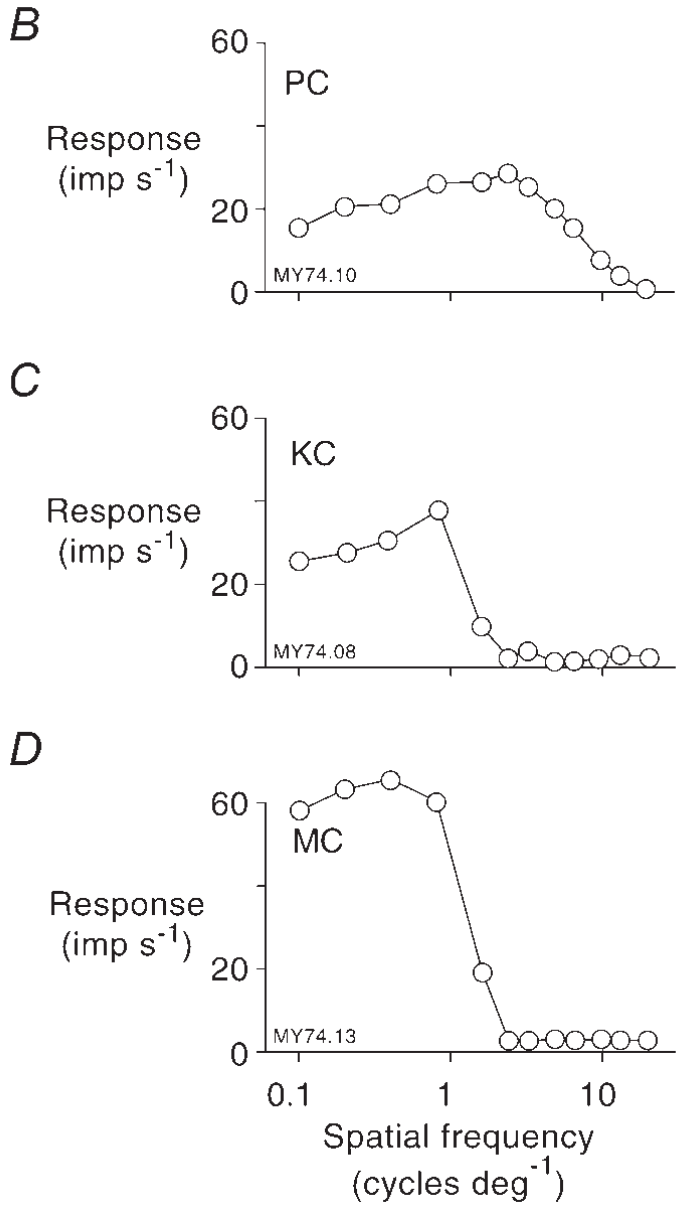

White, Solomon & Martin, 2001

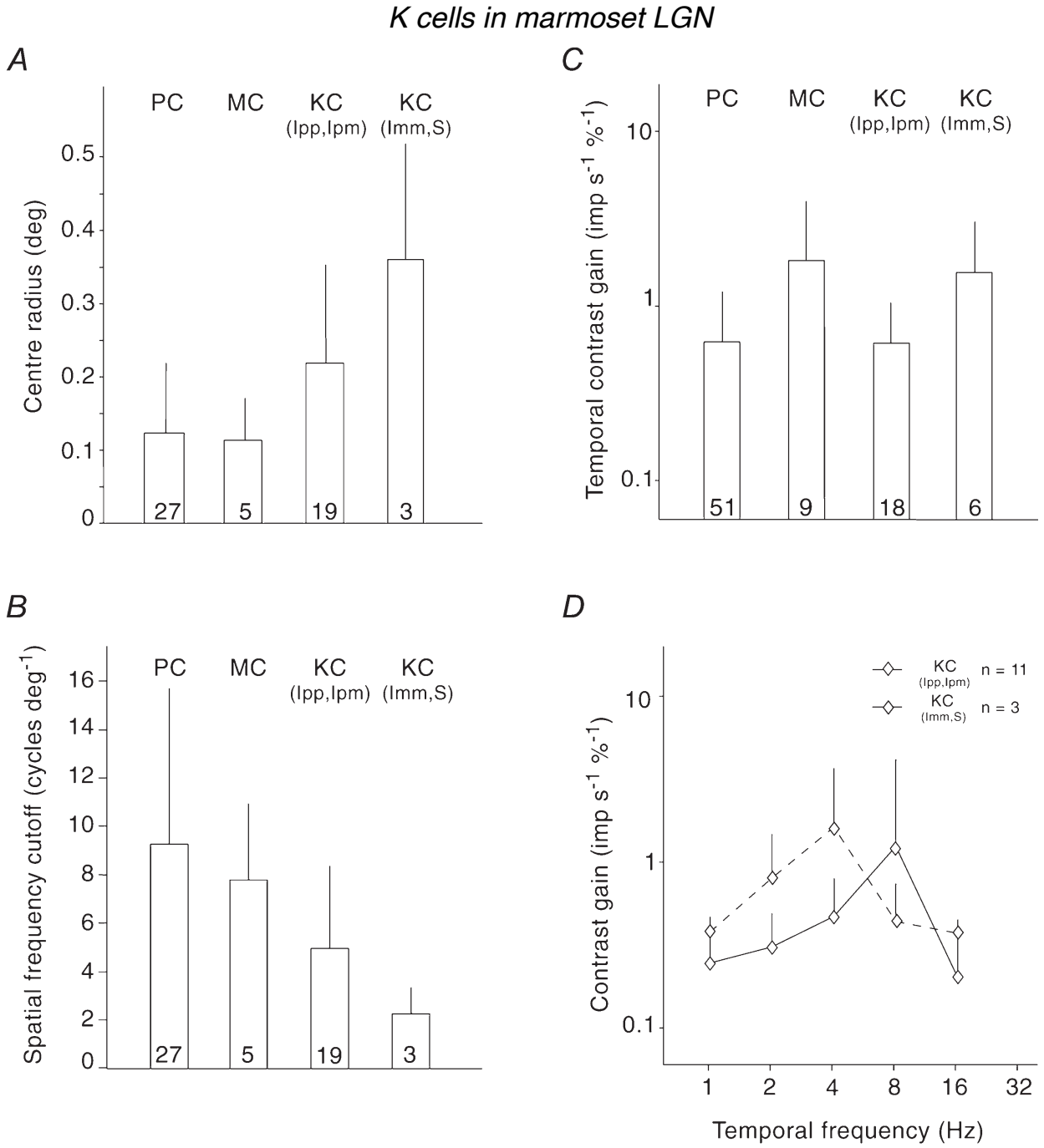

Figure 7. Summary of receptive field properties of KC cells, as compared to PC and MC cells

White, Solomon & Martin, 2001

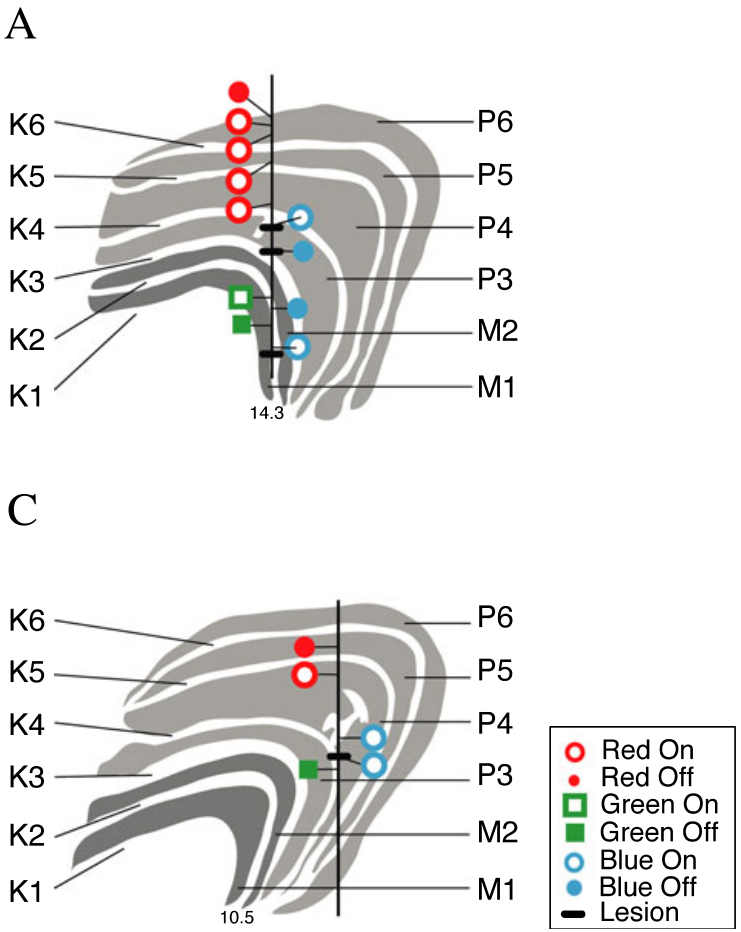

FIG 5. Electrode tracks, one from each of the four animals, with locations of the functionally identified cells, reconstructed from three or four Nissl-stained sections. The koniocellular extensions into the parvocellular layers (into P3 in A, B and D and P4 in C) near the electrode tracks are shown, but not all such koniocellular bridges in the sections are shown in the figure. The inset provides the key for cell types. The horizontal black lines on the electrode tracks indicate the sites of electrolytic lesions.

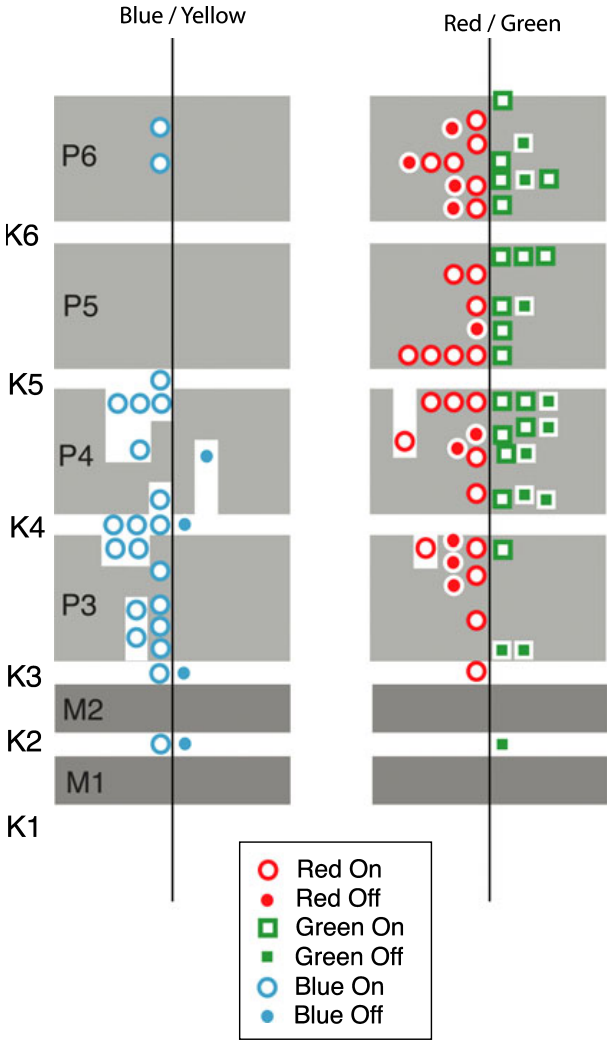

FIG 6. Pooled data of the laminar distribution of cell types within the LGN from all four monkeys (n = 88). The cells are placed along the schematised depth of the LGN, roughly proportionate to their distance from the immediately ventral koniocellular layer. In the left panel, the B/Y cells are shown with Blue On cells left of the vertical line and Blue Off cells to the right. In the right panel, R/G cells are shown with Red On and Red Off left of the vertical line and Green On and Green Off to the right. Where cells were localised in the koniocellular bridges in the parvocellular layers, such bridges are shown in the figure along with the cells localised within them. All except six cells (three R/G-opponent and three B/Y-opponent) were localized in the expected eye-specific layer.

The retina signals contrast

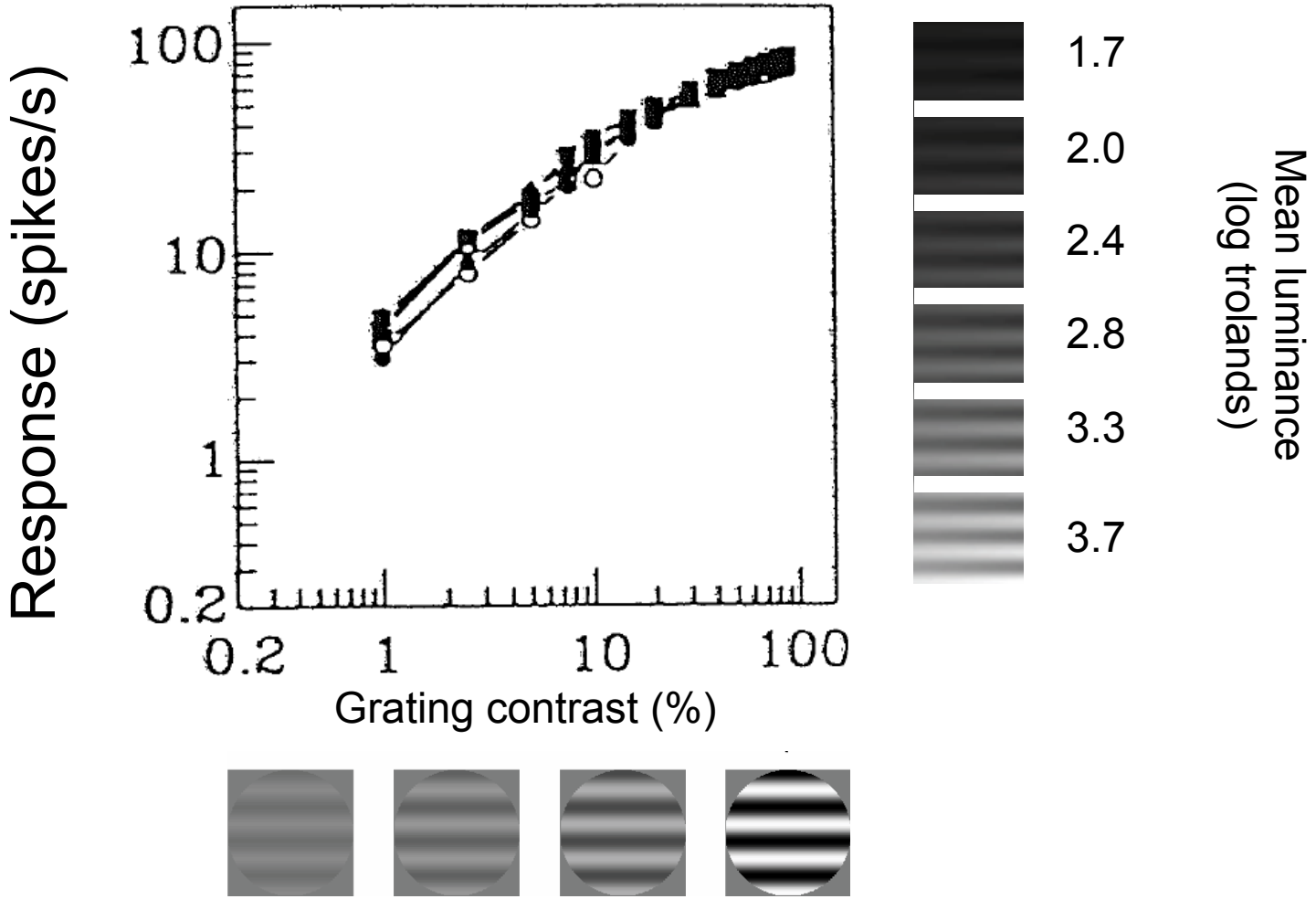

Troy and Enroth-Cugell, *Exp Brain Res,* 1993

The usefulness of adaptive responses

The usefulness of adaptive responses

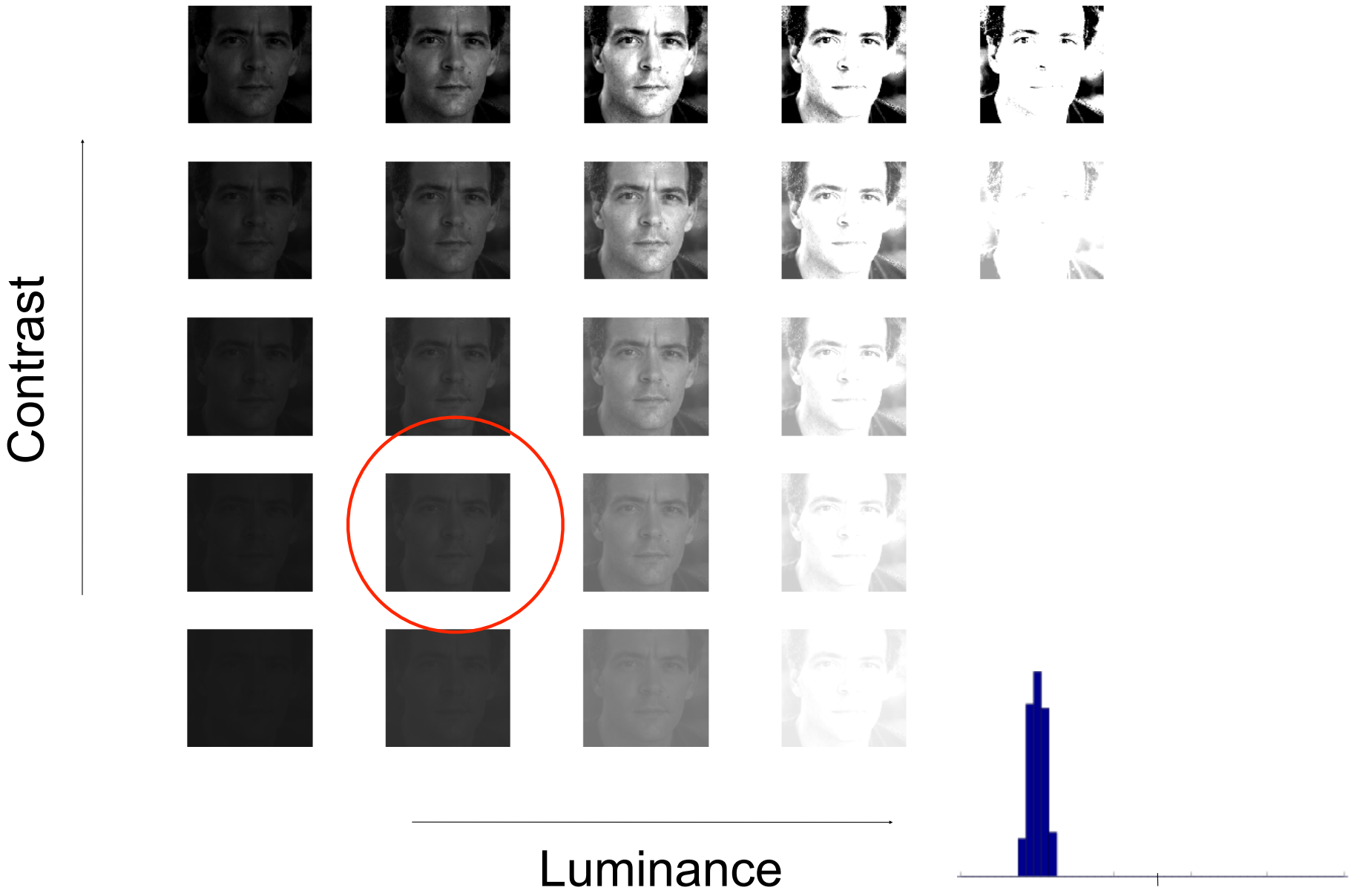

Adapt to luminance

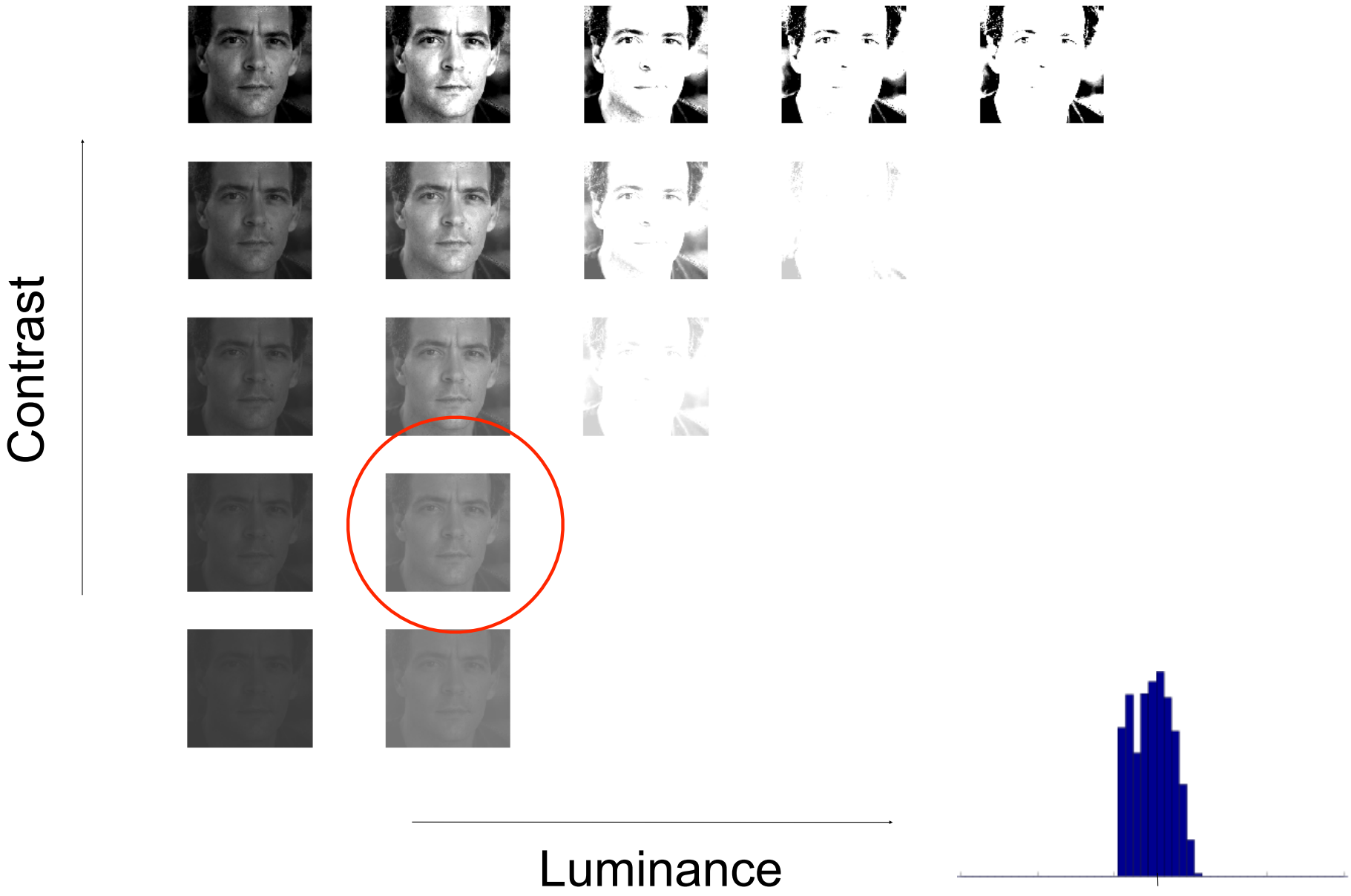

r.m.s contrast = standard deviation

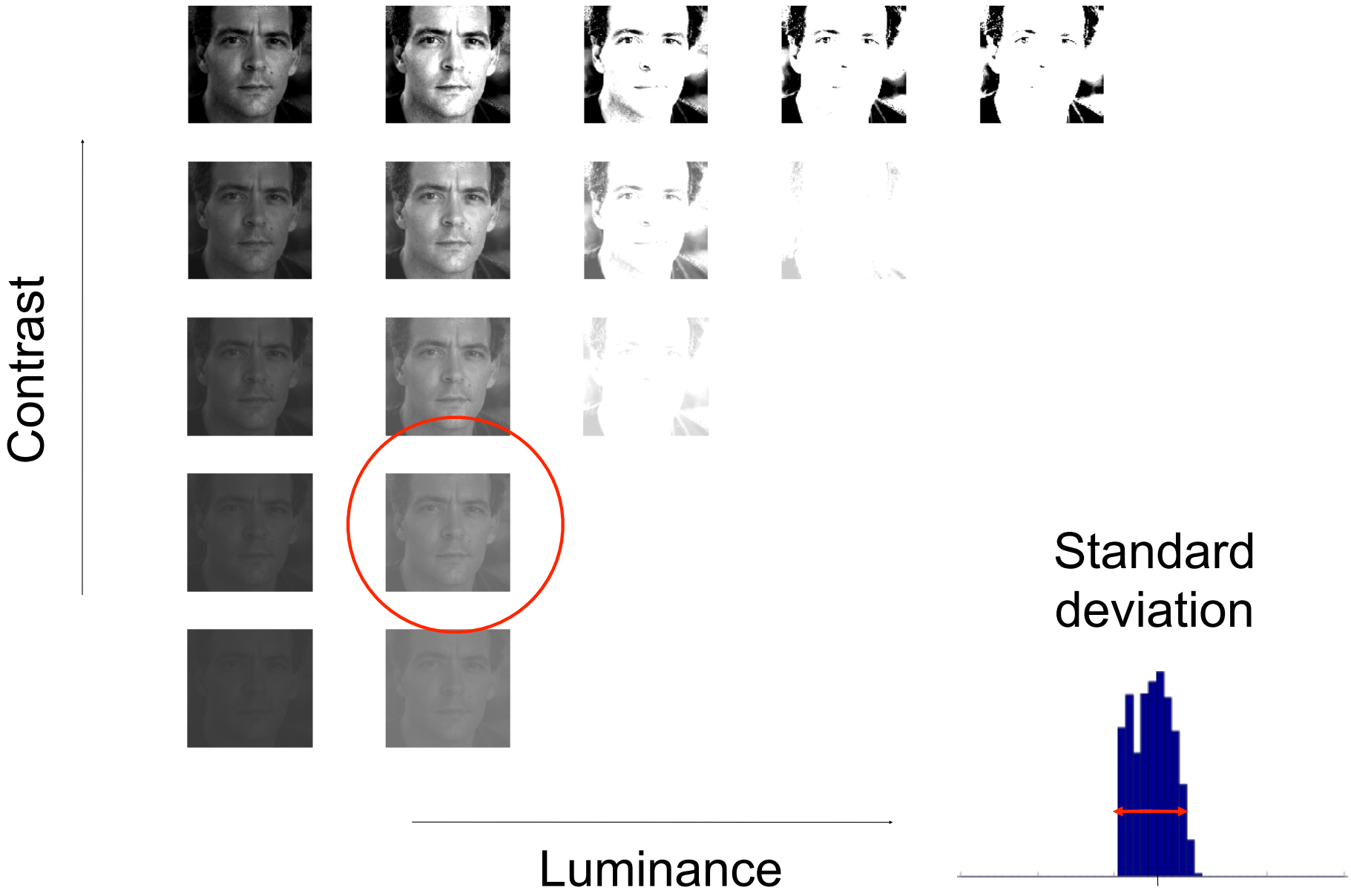

Adapt to contrast

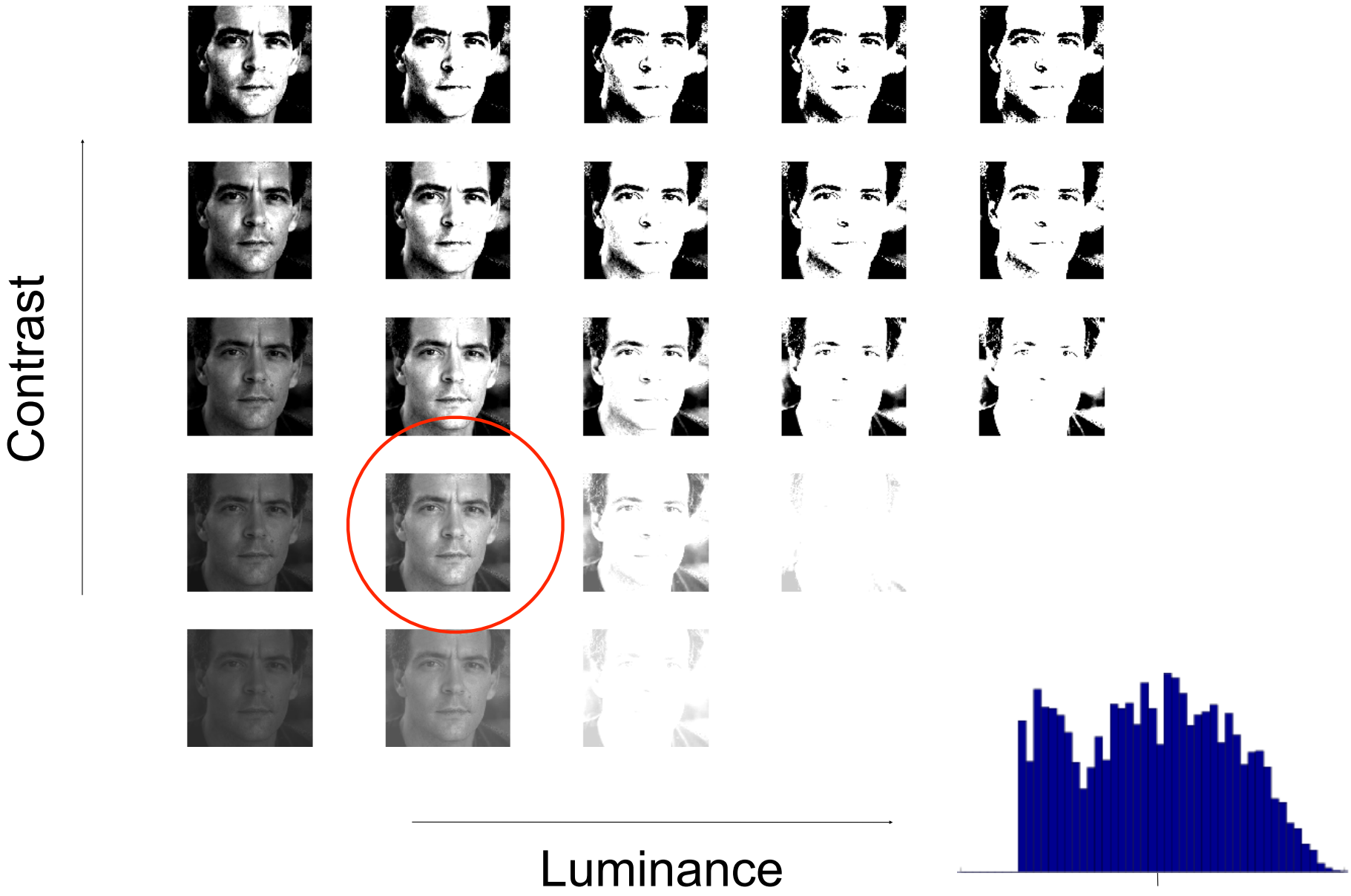

A model of light adaptation and contrast gain control

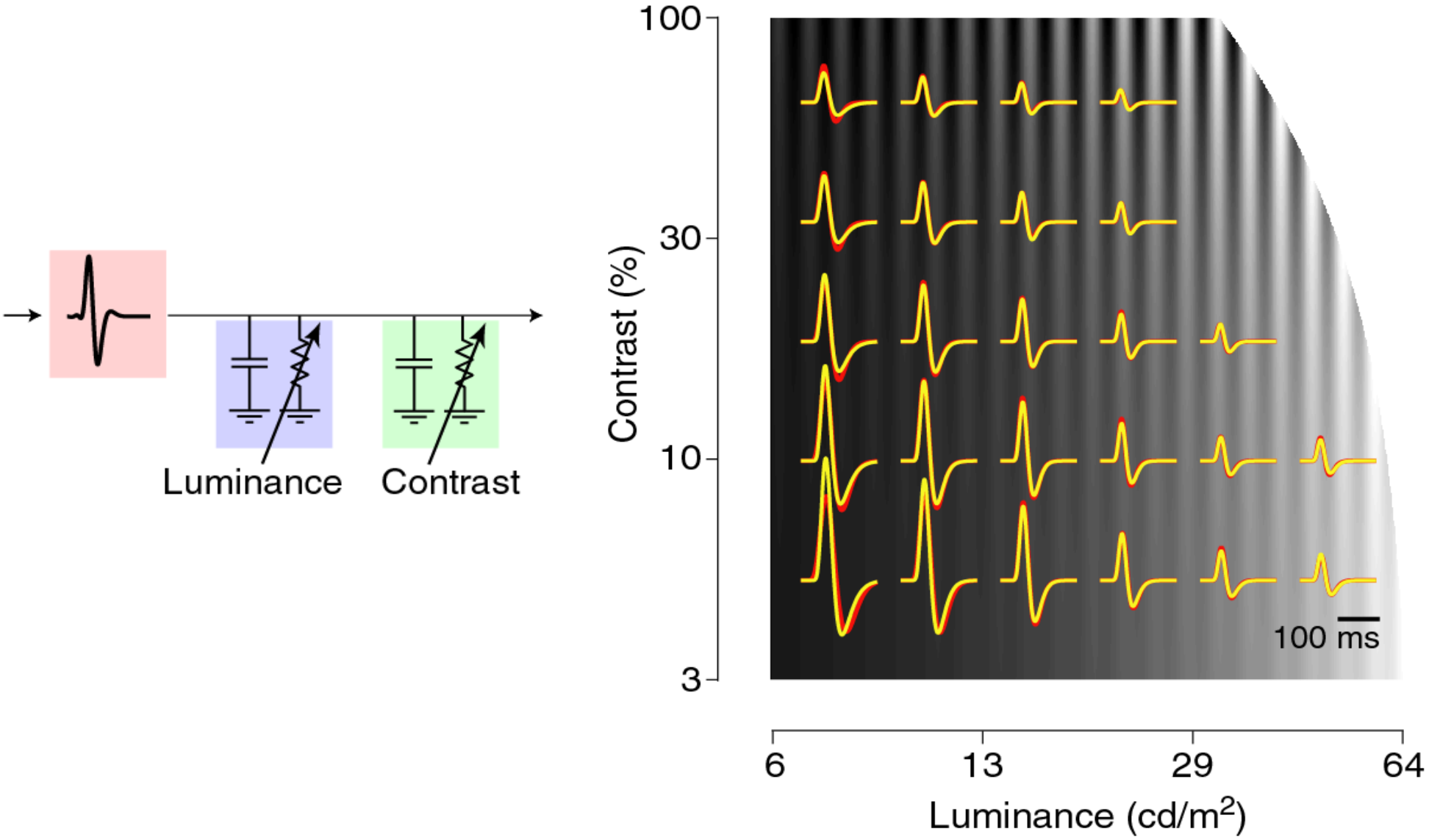

Mante, Bonin & Carandini, *Neuron,* 2008

A complete model

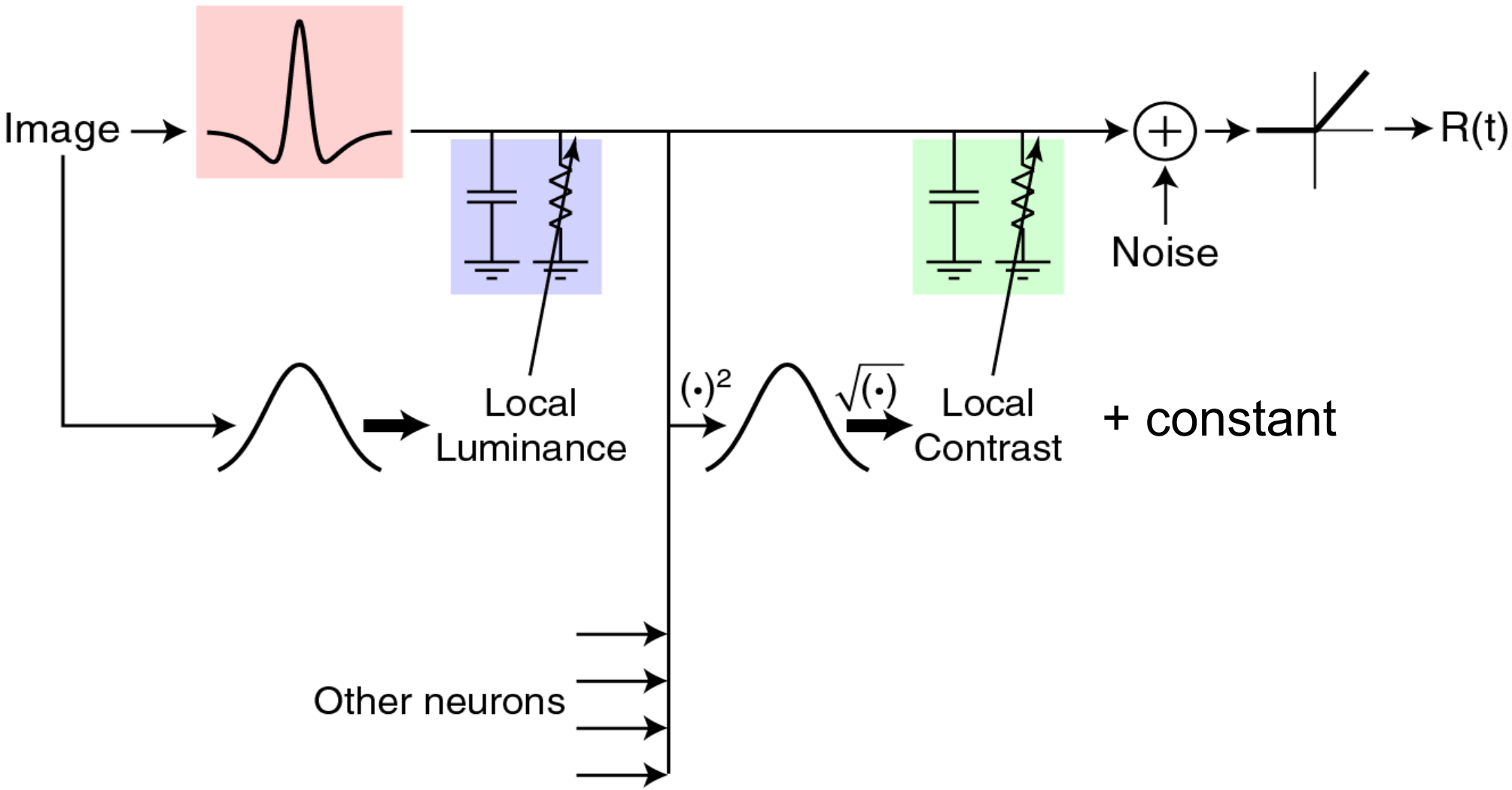

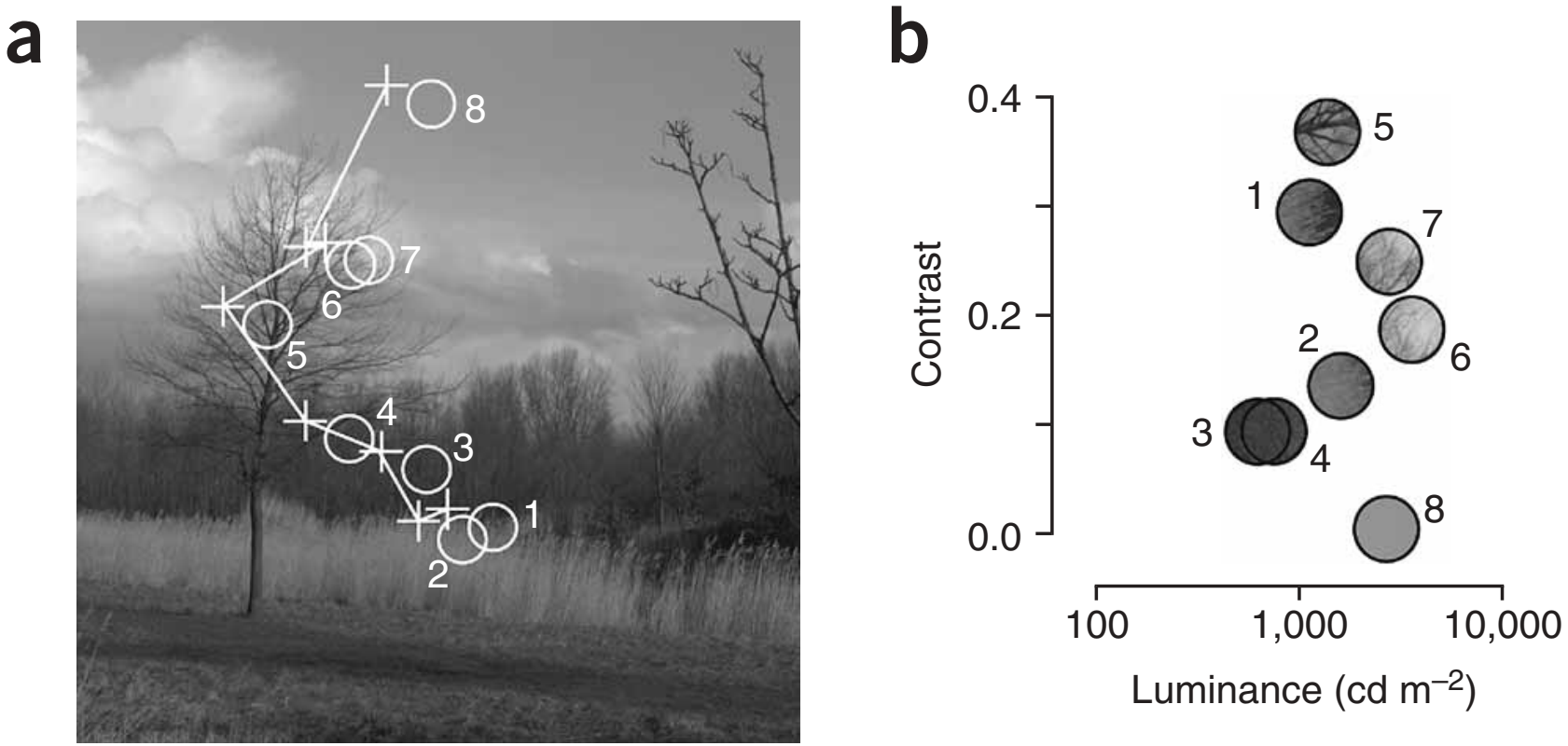

Figure 1 Luminance and contrast in a natural scene. (**a**) A sequence of fixations in a natural scene. The crosses indicate fixation locations and the circles represent the corresponding locations of an arbitrary receptive field (diameter: 1°). (**b**) Enlargements of the image patches falling within the receptive field as a function of their r.m.s. contrast (ordinate) and average luminance (abscissa).

Luminance and contrast vary independently in natural scenes

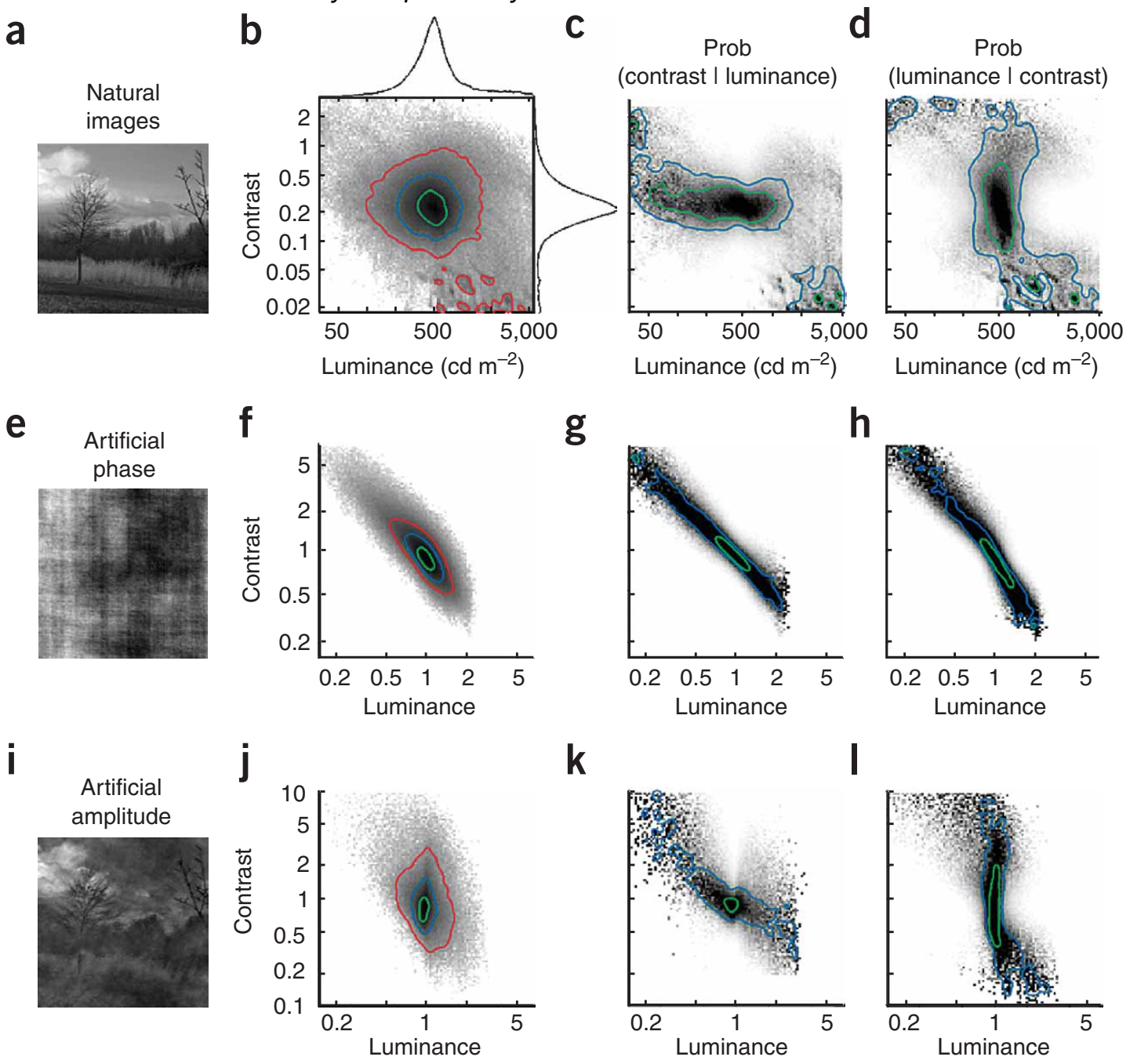

Figure 2 Statistics of local luminance and contrast in natural images. (**a**) A natural image (same as in **Fig. 1a**). (**b**) Joint distribution of luminance and contrast as sampled from all 300 images. These distributions represent the variation of luminance and contrast within a typical image: specifically, we first computed the overall average luminance and contrast across images, and then rescaled each image so that its average luminance and contrast would match the overall average. The contours delineate the regions containing 90% (red), 65% (blue) and 40% (green) of the observations. The curves on the sides of the joint distribution indicate the marginal distributions of luminance and contrast. (**c**) Conditional probability of observing a certain contrast given a specified luminance. This distribution is obtained by normalizing vertical slices of the joint distribution in **b**. (**d**) Conditional probability of observing a certain luminance given a specified contrast. This distribution is obtained by normalizing horizontal slices of the distribution in **b**. (**e**) An artificial-phase image. This image has the same amplitude spectrum as the image in **a**, but a random phase spectrum. (**f**–**h**). Joint distribution and conditional probability distributions for the 300 artificial-phase images. Format as in **b**–**d**. (**i**) An artificial-amplitude image. This image has the same phase spectrum as the image in **a**, but the amplitude at each frequency is given by the $1/f^n$ spectrum that best fits the spectrum of the original image. (**j**–**l**). Joint distribution and conditional probability distributions for the 300 artificial-amplitude images. Format as in **b**–**d**.

Mante et al (2005)

Light adaptation and contrast adaptation are very fast

Step in luminance

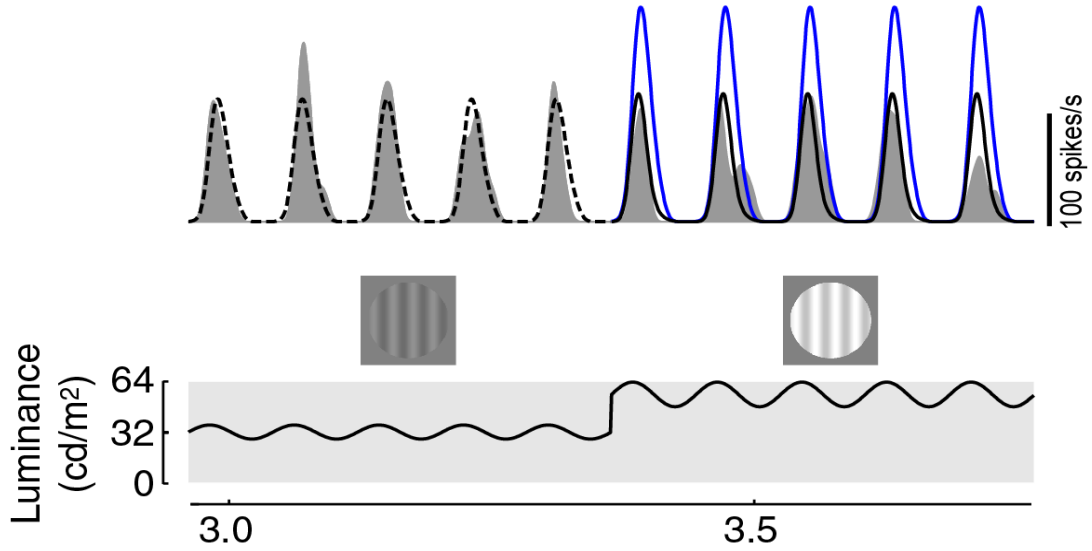

Step in contrast

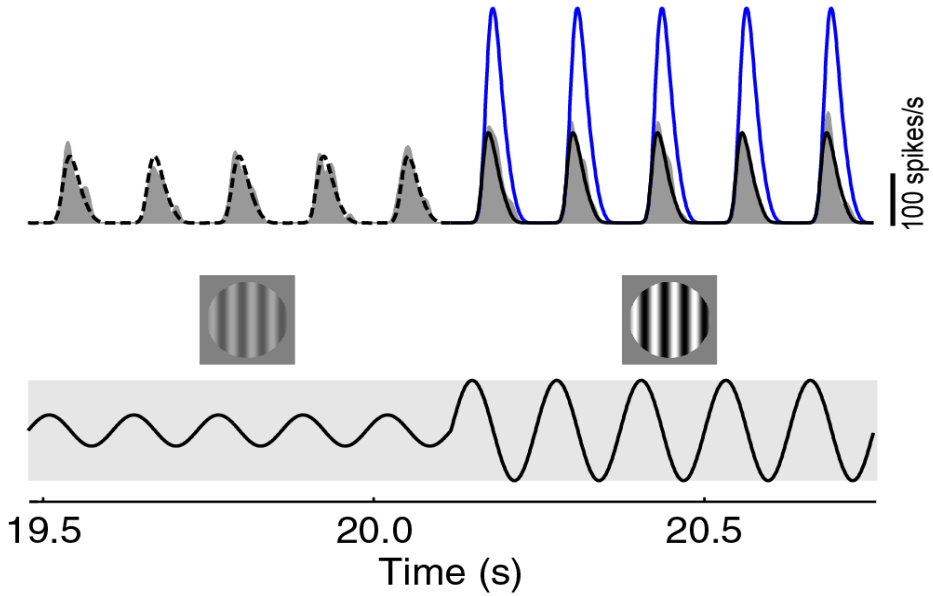

Mante, Frazor, Bonin, Geisler & Carandini, *Nature Neurosci,* 2005

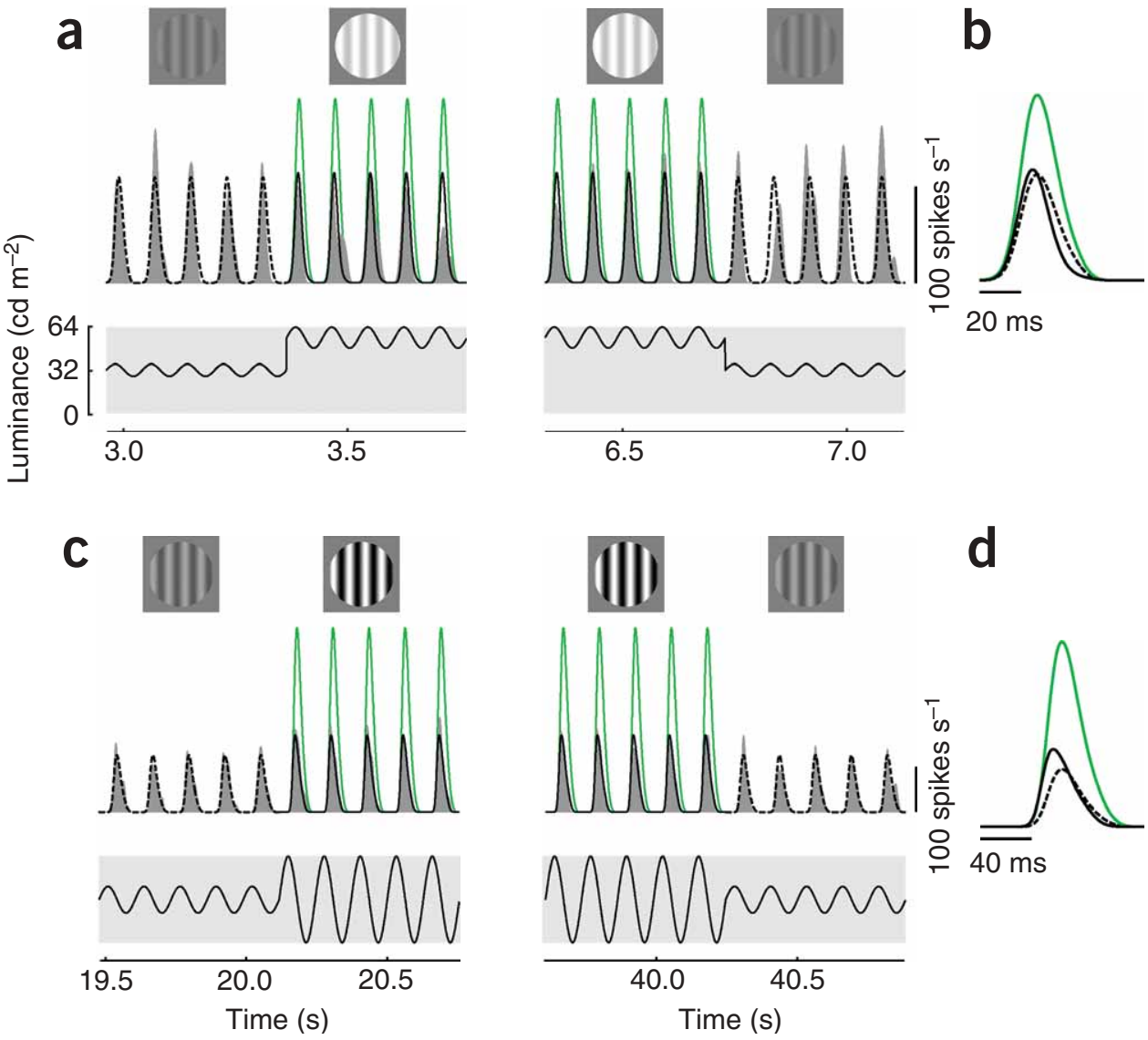

Figure 3 Effect and time course of gain control mechanisms in LGN. (**a**) Response of an LGN neuron to a drifting grating of constant contrast (14%), whose luminance steps from 32 cd m^{-2} to 56 cd m^{-2} (left) and back to 32 cd m^{-2} (right). Spatial frequency and temporal frequency (12.5 Hz) are optimal for this neuron. The temporal profile of the stimulus is shown below the responses. Histograms (gray) were obtained by convolving the spike trains with a Gaussian window ($\sigma = 5$ ms), and averaging over three stimulus presentations. From the histograms, we computed the average response to a cycle of the stimulus before (dashed) and after (black) the step in luminance. The linear prediction (green) was obtained by scaling the response before the step (dashed) by the ratio of the two luminances. (**b**) Comparison of average responses to low luminance (dashed) and high luminance (black), and of the response expected in the absence of gain control (green). (**c**) Response of an LGN neuron to a drifting grating of constant luminance (32 cd m^{-2}) whose contrast steps from 31% to 100% (left) and back to 31% (right). Spatial frequency and temporal frequency (7.8 Hz) are optimal for this neuron. Histograms (gray) are the average over five stimulus presentations. The linear prediction (green) was obtained by scaling the response before the step (dashed) by the ratio of the two contrasts. (**d**) Comparison of average responses to low contrast (dashed) and high contrast (black), and of the response expected in the absence of gain control (green).

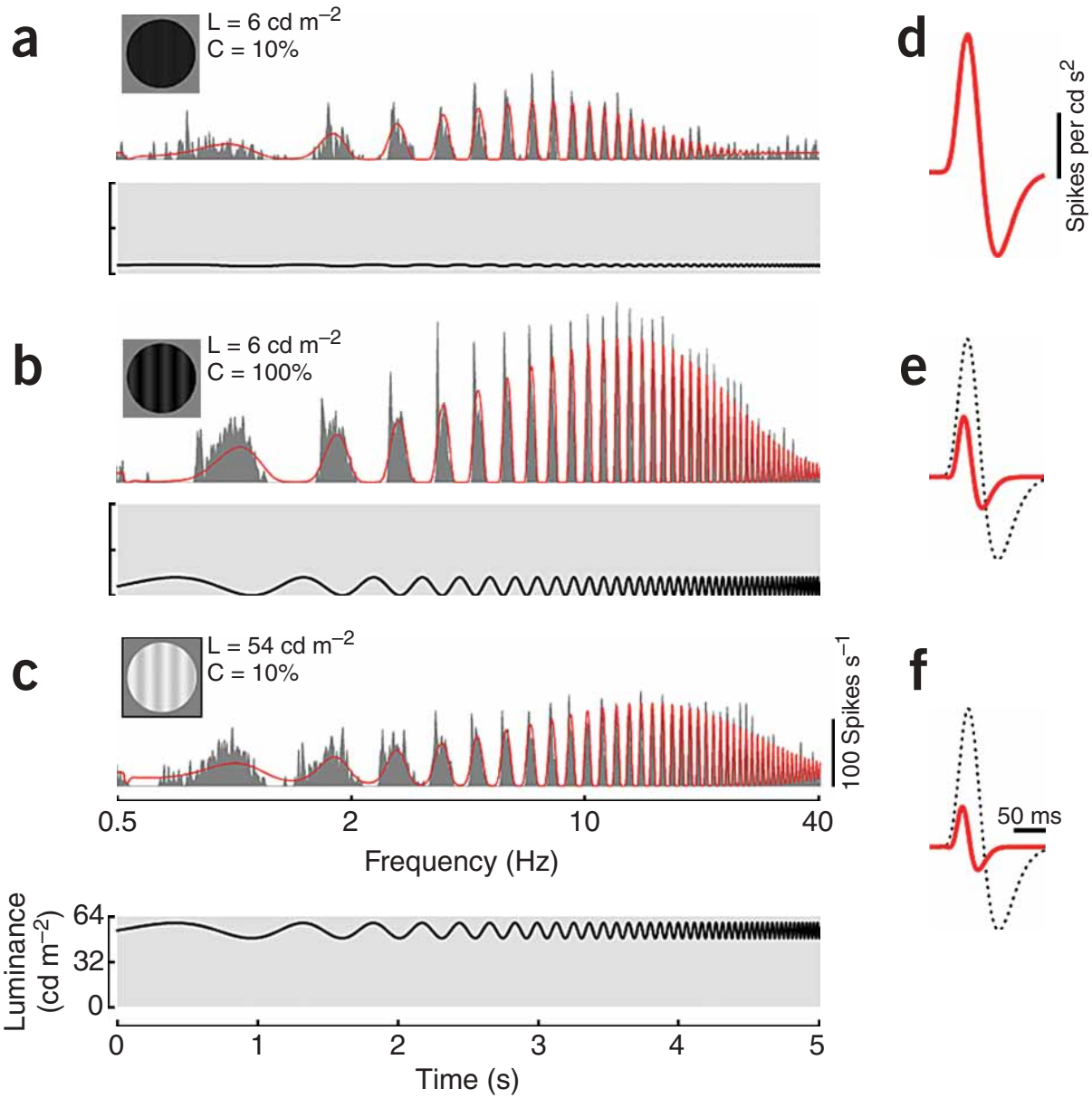

Figure 4 Characterizing LGN responses at various luminances and contrasts. (**a**–**c**) Responses of an LGN neuron (X-type, on-center) to temporal frequency sweeps at (**a**) low luminance and low contrast ($L = 6$ cd m^{-2}, $C = 10\%$, Michelson contrast), (**b**) low luminance and high contrast ($L = 6$ cd m^{-2}, $C = 100\%$) and (**c**) high luminance and high contrast ($L = 54$ cd m^{-2}, $C = 10\%$). Histograms (gray) were obtained by averaging over ten stimulus presentations. Red curves are descriptions of the responses by the descriptive model (**Fig. 5a**). Stimuli were sinusoidal gratings at optimal spatial frequency (icons). The temporal profile of the stimuli is shown under the responses; drift rate increased exponentially with time, from 0.5 Hz to 40 Hz in 5 s, and back (not shown). (**d**–**f**) Impulse responses used for the predictions in **a**–**c**. The impulse response is smaller and faster at the higher contrast (**e**) or luminance (**f**) than at low luminance and contrast (**d**, and dotted curves).

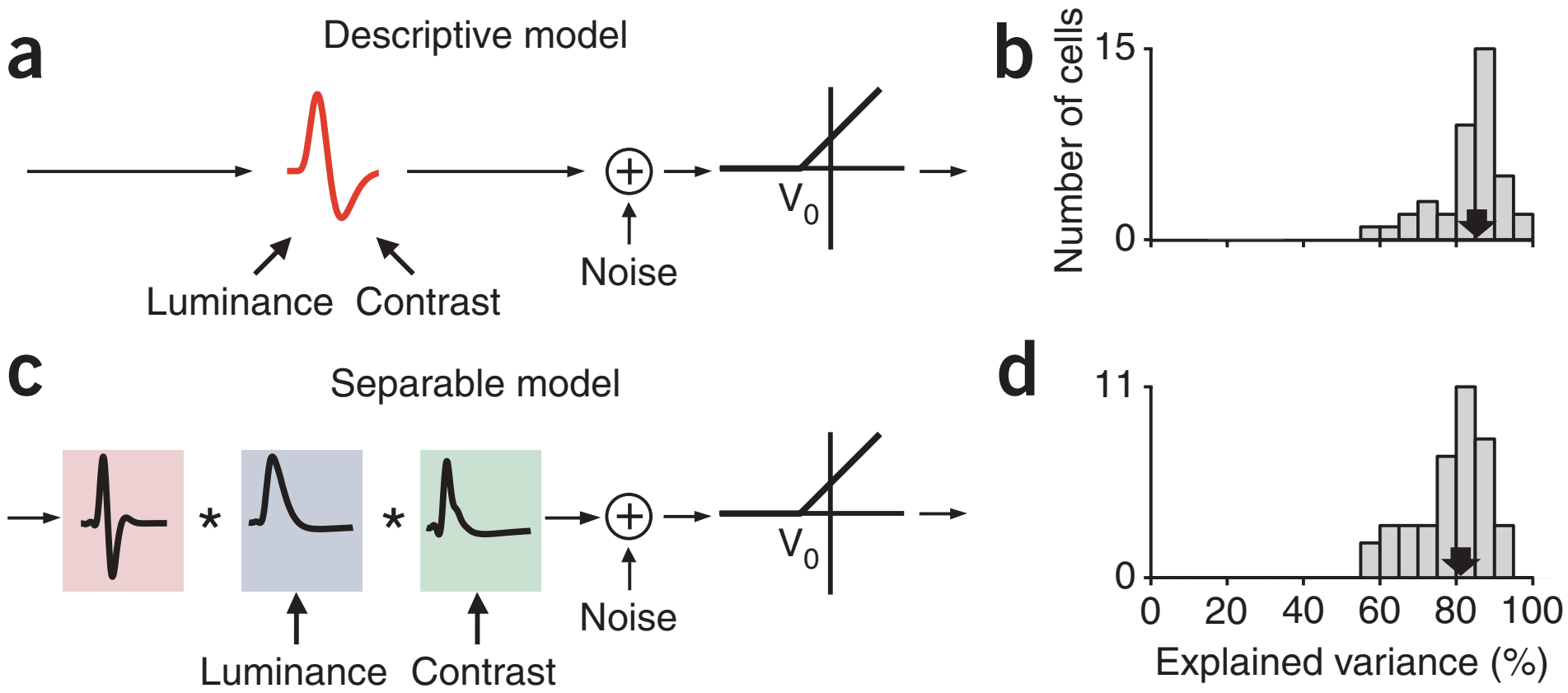

Figure 5 The two models used to describe LGN responses, and a measure of their performance. (**a**) The descriptive model: stimulus luminance is integrated by the spatial receptive field, filtered by the impulse response (red), added to Gaussian noise and rectified. (**b**) Quality of predictions for the descriptive model, measured by the percentage of stimulus-driven response variance explained by the model. $N = 40$. The median is 85% (arrow). (**c**) The separable model. The impulse response is the convolution of three filters: a fixed filter (pink), a luminance gain filter (blue) and a contrast gain filter (green). (**d**) Quality of predictions for the separable model. The median explained variance is 81% (arrow).

Mante et al (2005)

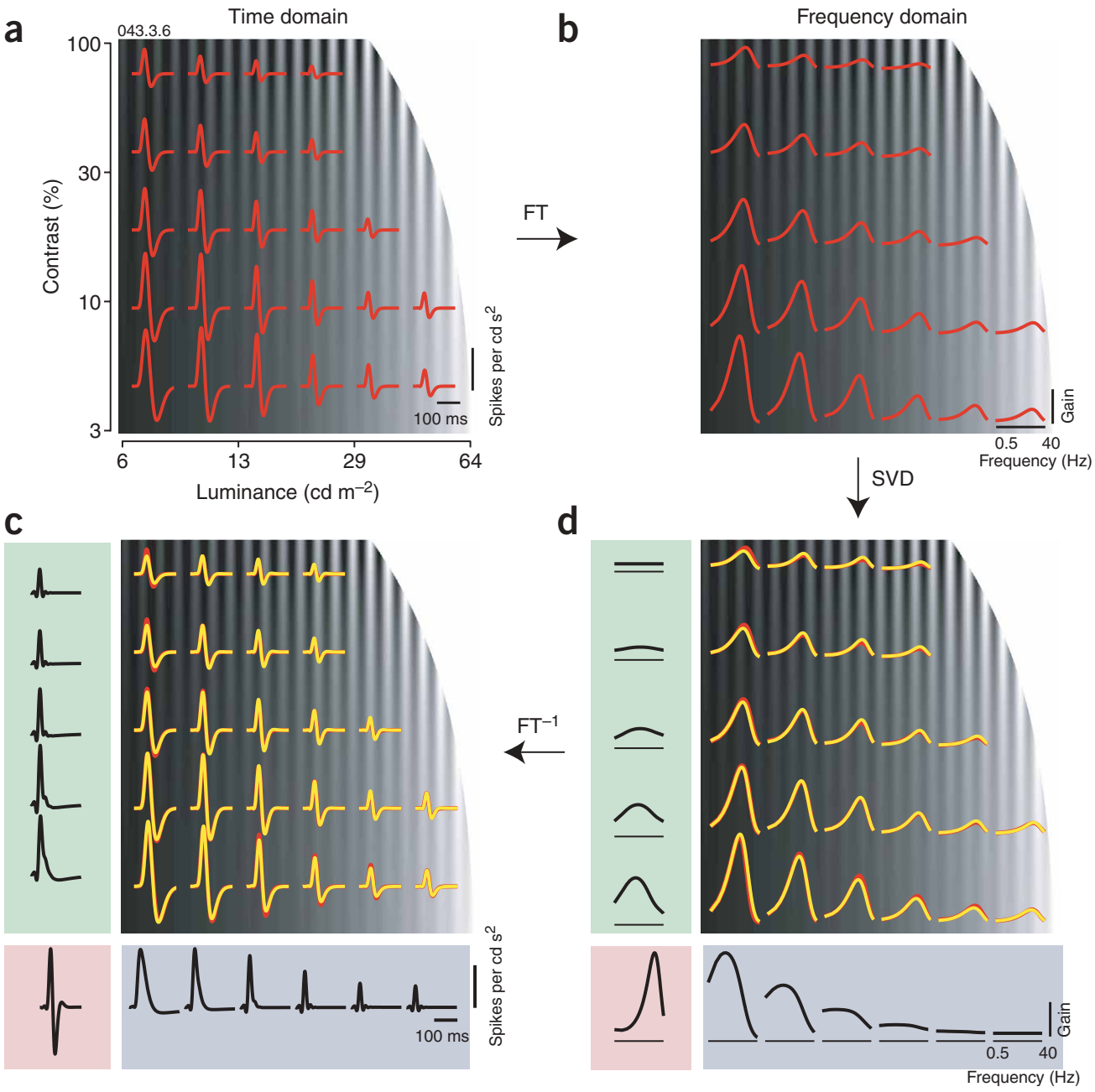

Figure 6 Independence of the effects of luminance gain control and contrast gain control. (**a**) Impulse responses of the cell in **Figure 4**, measured by fitting the descriptive model for all combinations of mean luminance and contrast. (**b**) The amplitude of the transfer functions corresponding to those impulse responses, as a function of frequency. (**c**) Impulse responses predicted by the separable model (yellow), compared to those predicted by the descriptive model (red, replotted from **a** for comparison). The latter are barely visible in the superposition, indicating that the predicted impulse responses are extremely similar. Each impulse response (yellow) is the convolution of the fixed filter (pink) with the luminance gain filter in the appropriate column (blue) and a contrast gain filter in the appropriate row (green). (**d**) The amplitude transfer functions corresponding to those impulse responses, as a function of frequency. The arrows between the panels indicate the sequence of operations: Fourier transform (FT, **a** to **b**), singular value decomposition (SVD, **b** to **d**), and inverse Fourier transform (FT^{-1}, **d** to **c**).

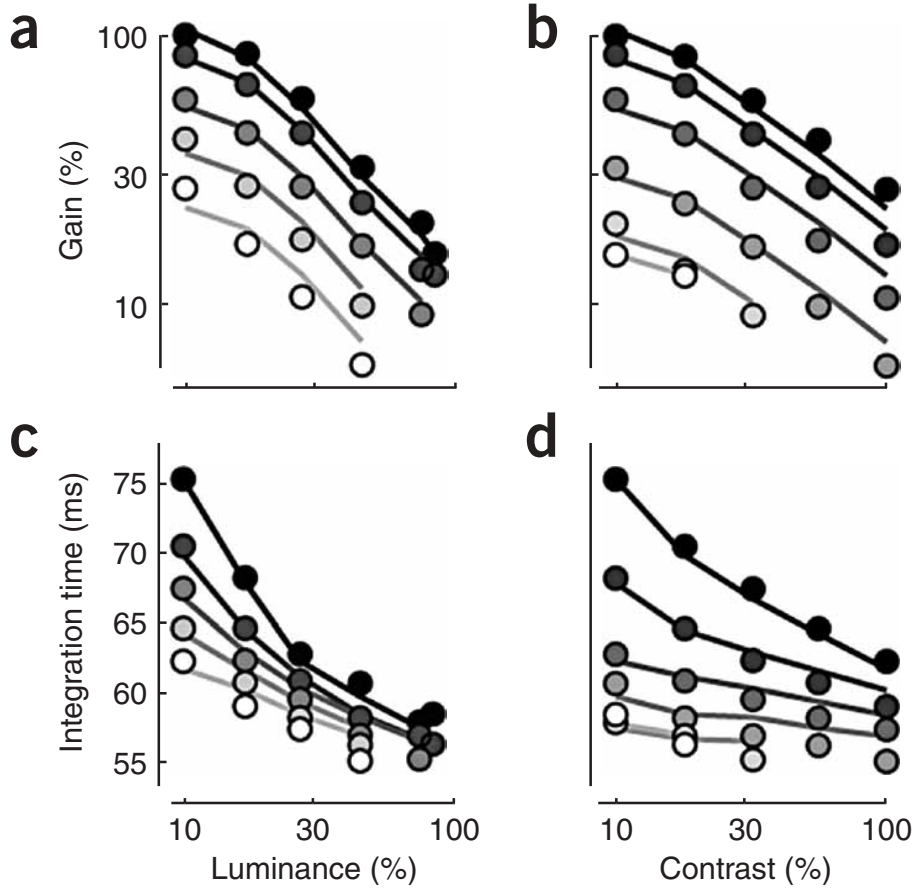

Figure 7 Summary of the effects of luminance and contrast, and predictions of the separable model. Data points indicate the overall gain (top) and integration time (bottom) for the data of **Figure 6**. Lines show the predictions of the separable model. (**a**) Overall gain as a function of mean luminance, for different contrasts (black to white: 10% to 100%). (**b**) Gain replotted as a function of contrast, for different mean luminances (black to white: 10% to 84%). (**c**) Overall integration time as a function of luminance, for different contrasts (as in **a**). (**d**) Integration time as a function of contrast, for different luminances (as in **b**).

Mante et al (2005)

Projections of the retina

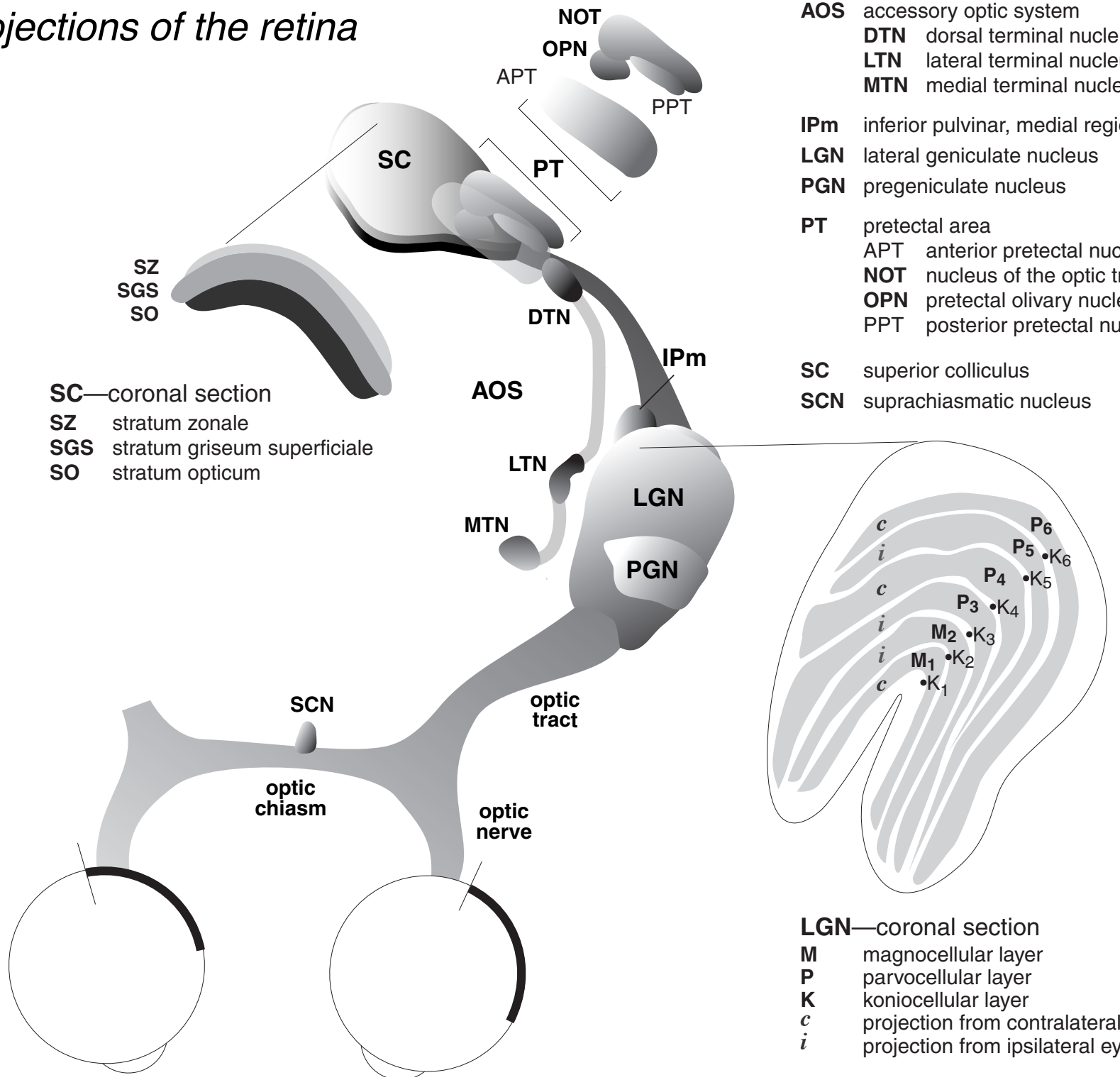

AOS accessory optic system
- **DTN** dorsal terminal nucleus
- **LTN** lateral terminal nucleus
- **MTN** medial terminal nucleus

IPm inferior pulvinar, medial region

LGN lateral geniculate nucleus

PGN pregeniculate nucleus

PT pretectal area
- APT anterior pretectal nucleus
- **NOT** nucleus of the optic tract
- **OPN** pretectal olivary nucleus
- PPT posterior pretectal nucleus

SC superior colliculus

SCN suprachiasmatic nucleus

SC—coronal section
- **SZ** stratum zonale
- **SGS** stratum griseum superficiale
- **SO** stratum opticum

LGN—coronal section
- **M** magnocellular layer
- **P** parvocellular layer
- **K** koniocellular layer
- *c* projection from contralateral eye
- *i* projection from ipsilateral eye

Superior colliculus

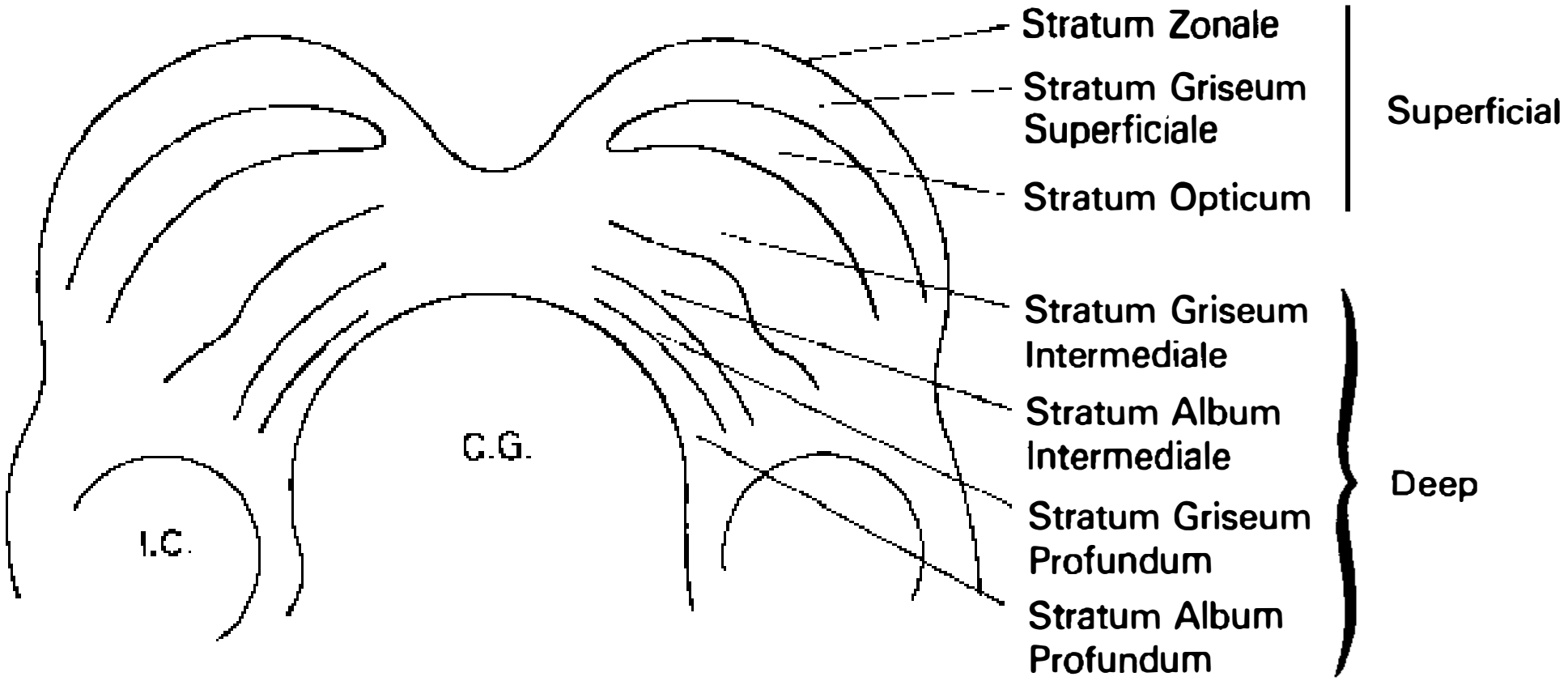

Figure 1 Alternating fiber and cell layers of monkey superior colliculus. A drawing of a coronal section through the colliculus is shown. The seven layers indicated on the right are divided into three layers designated as the superficial division and four layers designated as the deep division. I. C., inferior colliculus; C. G., central gray.

Superior colliculus

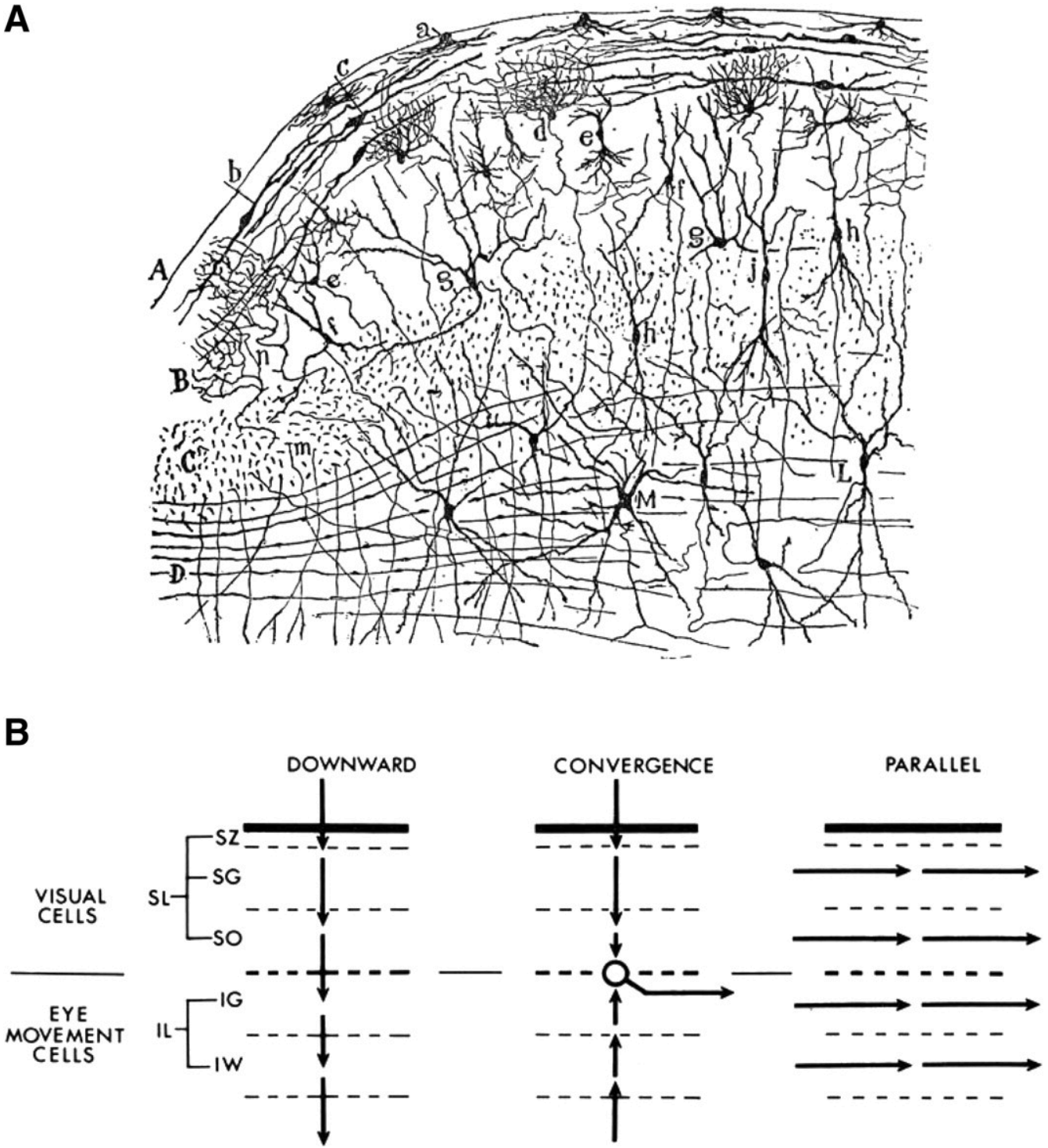

Two Visual Systems

Brain mechanisms for localization and discrimination are dissociated by tectal and cortical lesions.

Gerald E. Schneider

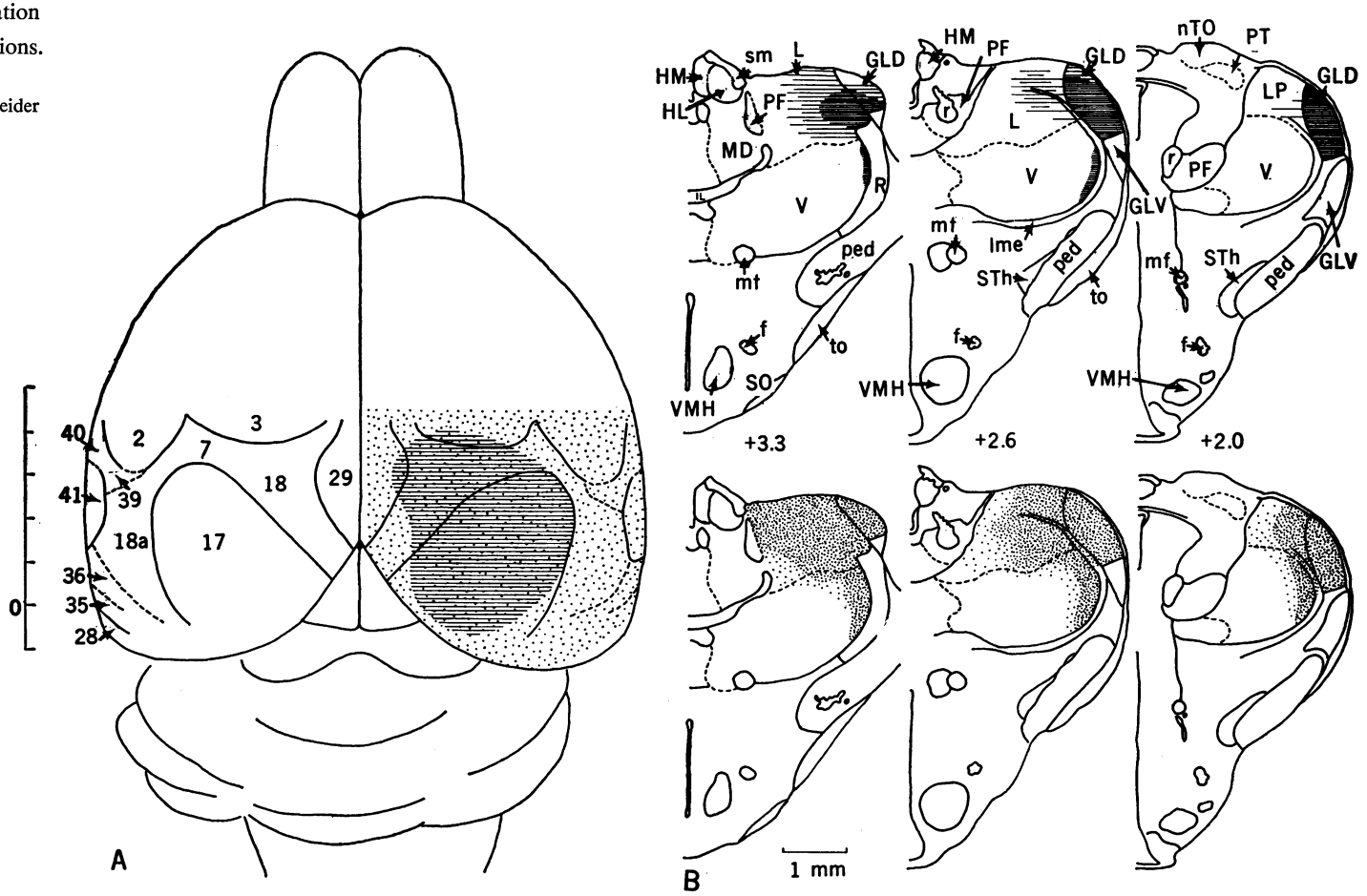

Fig. 2. (A) Dorsal view of hamster brain drawn to scale. (Left side) Fiber-architectonic map of visual areas (*31*); the numbering is Krieg's for the rat (*32*). Dashed lines indicate difficulty in consistent delineation; absence of border, as between areas 7 and 18, indicates that there were no sharp changes in histological appearance in the 25-micron frontal sections used. (Right side) Outlines of largest and smallest neocortical lesions. The horizontal bars cover the lesion of most of areas 17 and 18; the placement of the lesion was based on an early mapping of visual cortex by cytoarchitecture (appearance and organization of cell bodies). The scale is in millimeters; the lambda point serves as the zero reference in the anterior-posterior plane. The brain is correctly aligned when the skull is leveled by placing the bregma and the occipitointerparietal suture at equal elevations. (B) Drawings of frontal sections through the thalamus below a cortical lesion showing typical patterns of partial retrograde degeneration following the smallest type (top) and largest type of lesion. Density of stippling or lines corresponds to severity of degeneration. Not shown is the partial degeneration usually found in the anteroventral nucleus and, in the case of the largest type of lesion, in the medial geniculate nucleus. Dashed lines indicate divisions difficult to delineate. (*HL*) Lateral habenular nucleus; (*HM*) medial habenular nucleus; (*f*) fornix; (*GLD*) dorsal lateral geniculate nucleus; (*GLV*) ventral lateral geniculate nucleus; (*IL*) intralaminar nuclei; (*L*) lateral nucleus; (*lme*) external medullary lamina; (*LP*) lateral posterior nucleus; (*MD*) medial dorsal nucleus; (*mt*) mamillothalamic tract; (*nTO*) nucleus of the optic tract; (*ped*) cerebral peduncle; (*PF*) parafascicular nucleus; (*PT*) pretectal nucleus; (*r*) fasciculus retroflexus; (*R*) reticular nucleus; (*sm*) stria medullaris; (*SO*) supraoptic nucleus; (*STh*) subthalamic nucleus; (*to*) optic tract; (*V*) ventral nucleus; (*VMH*) ventromedial nucleus of the hypothalamus.

Two Visual Systems

Brain mechanisms for localization and discrimination are dissociated by tectal and cortical lesions.

Gerald E. Schneider

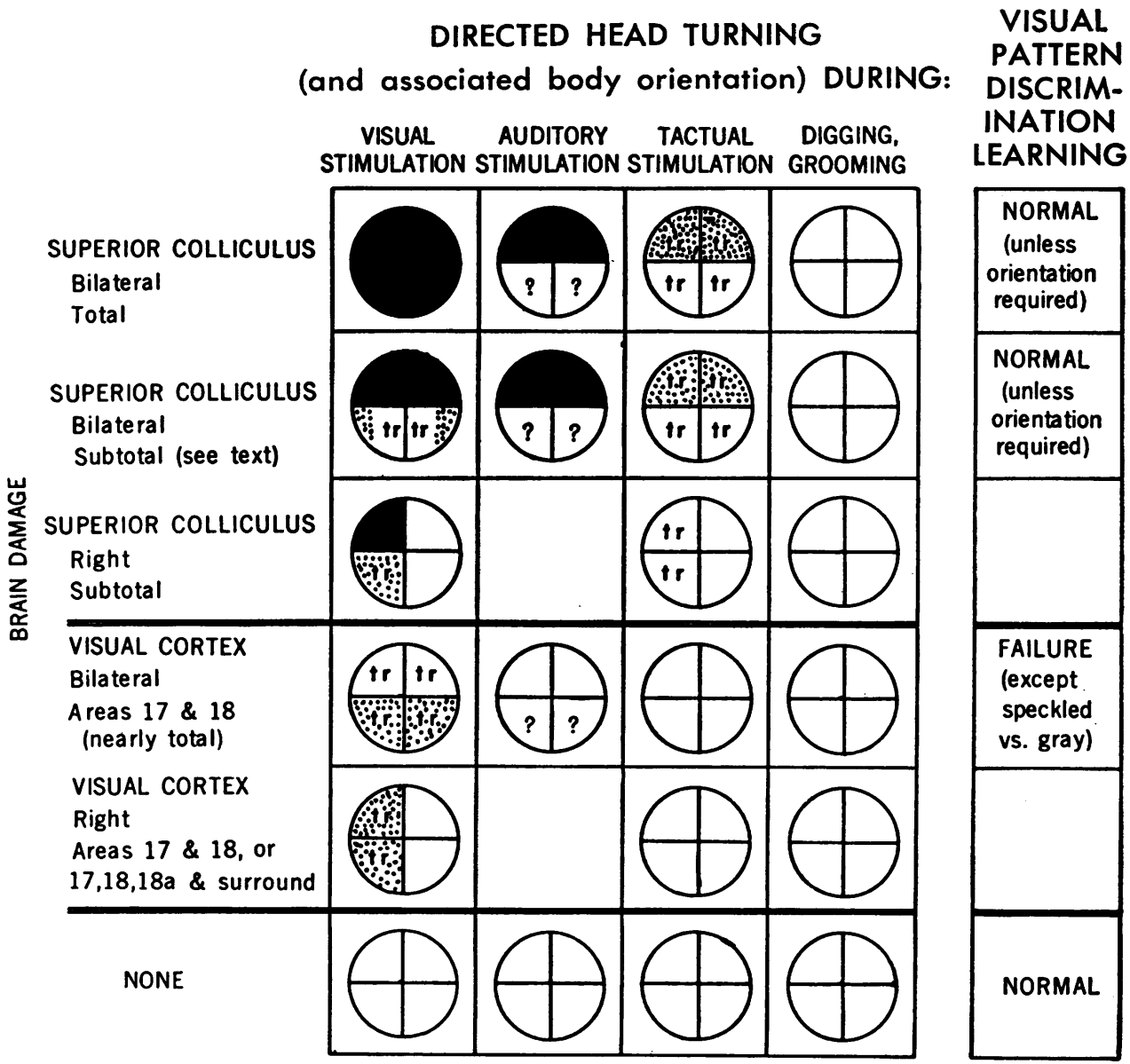

Fig. 3. Diagrams showing the abilities of hamsters with various types of brain damage to turn the head toward the left or right (lower quadrants of circles), or raise the head (upper quadrants) in response to the type of stimulation indicated at top of column: (black quadrant) failure to turn; (stippling) turns, but fewer than normal; (*tr*) transient deficit or failure; (?) not tested. At the far right, results on the visual discrimination tests are summarized.

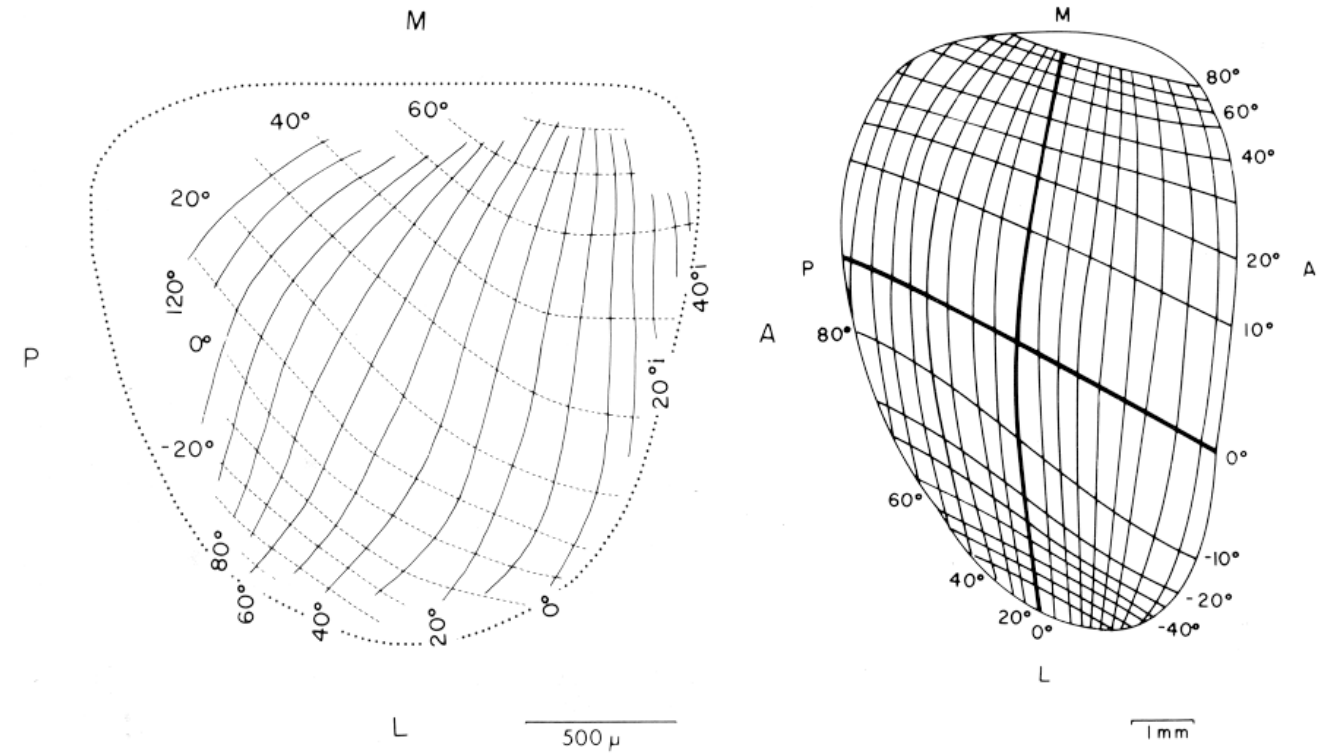

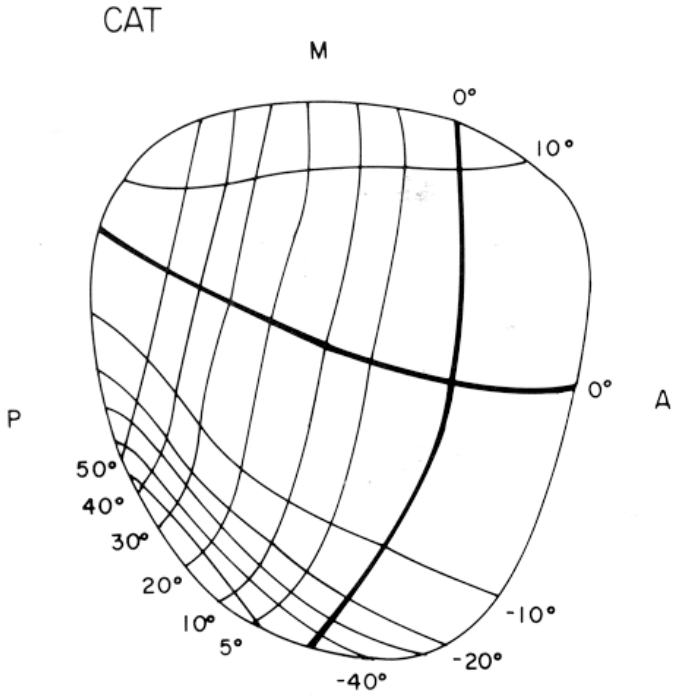

FIG. 5. Topographic layout of visual field on surface of superior colliculus of mouse, rabbit, and cat. Derivation of 0° vertical meridian is different in each of these maps. In the mouse map the 0° vertical meridian is the vertical plane that intersects the projection of the long axis of the mouse's head. In the rabbit map the 0° vertical meridian intersects the perpendicular to the long axis of the head, which passes through the corneal vertex. In the cat map the 0° vertical meridian intersects the projection line of area centralis. In all three maps the 0° horizontal meridian intersects each of the described projection lines in the horizontal plane. Horizontal meridians run in the antero-posterior direction. The maps represent the contralateral retinal projection. A, anterior; P, posterior; M, medial; L, lateral. [Mouse data from Dräger and Hubel (44); rabbit data from Hughes (108); cat diagram courtesy of H. Sherk from data of Berman and Cynader (21) and Feldon et al. (53).]

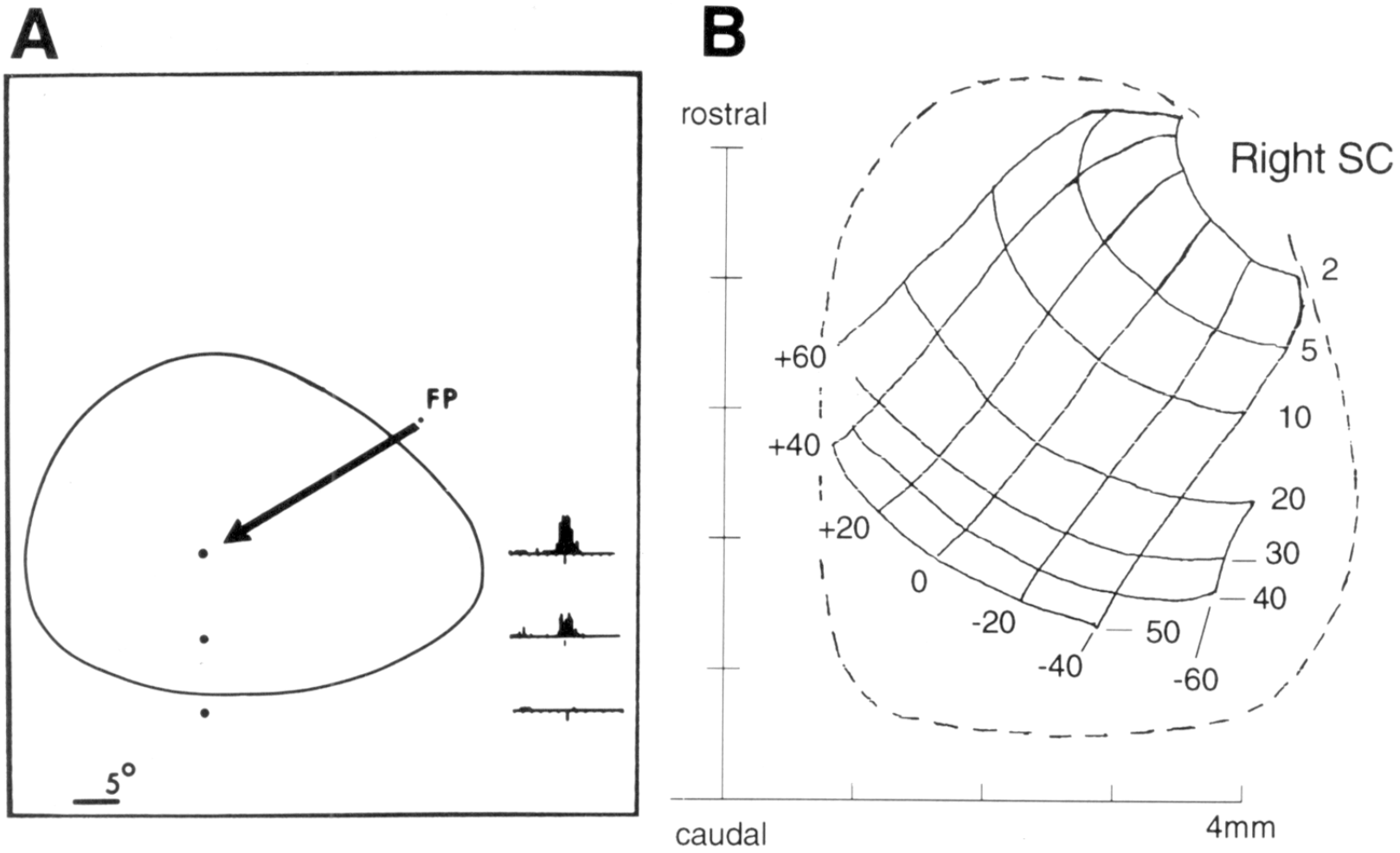

FIGURE 4. (**A**) Schematic drawing of the screen on which the monkey fixates and the fixation point (FP) that goes off as the target (*dot*) comes on. When the monkey makes a saccade to the target, the cell discharge increases if the saccade is to the center of the movement field (*top histogram*), and it increases less before saccades to other targets. (**B**) Schematic map of the intermediate layers of the monkey superior colliculus. The map of the amplitude and direction of saccades was made by electrically stimulating the colliculus. Modified from Robinson DA. Eye movements evoked by collicular stimulation in the alert monkey. *Vision Res.* 1972;12:1795–1808.

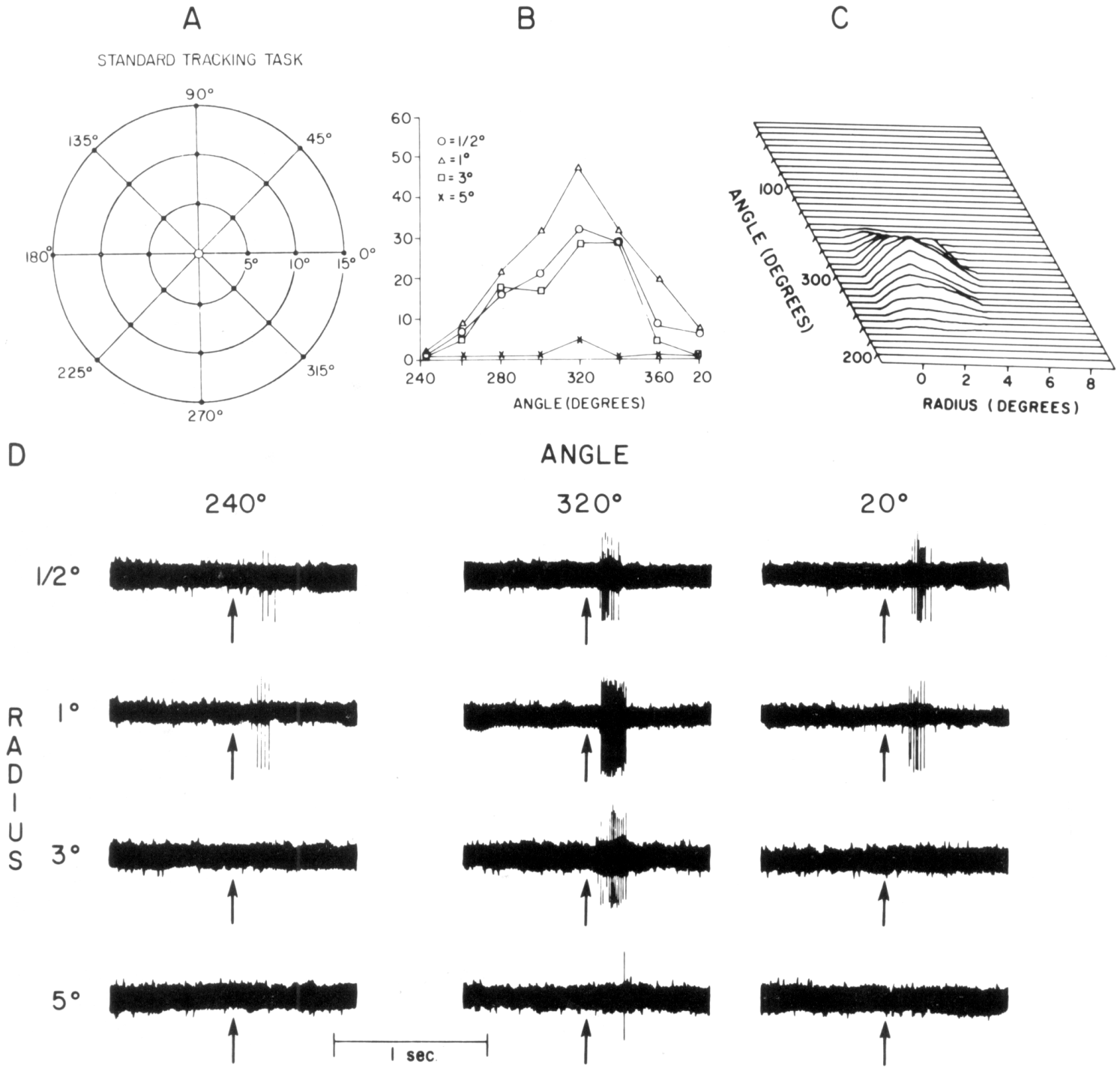
A
STANDARD TRACKING TASK
90°
135°
45°
180°
0°
225°
315°
270°
5°
10°
15°
B
○ = 1/2°
△ = 1°
□ = 3°
x = 5°
60
50
40
30
20
10
0
240
280
320
360
20
ANGLE (DEGREES)
C
ANGLE (DEGREES)
100
300
200
0
2
4
6
8
RADIUS (DEGREES)
D
ANGLE
240°
320°
20°
RADIUS
1/2°
1°
3°
5°
1 sec.

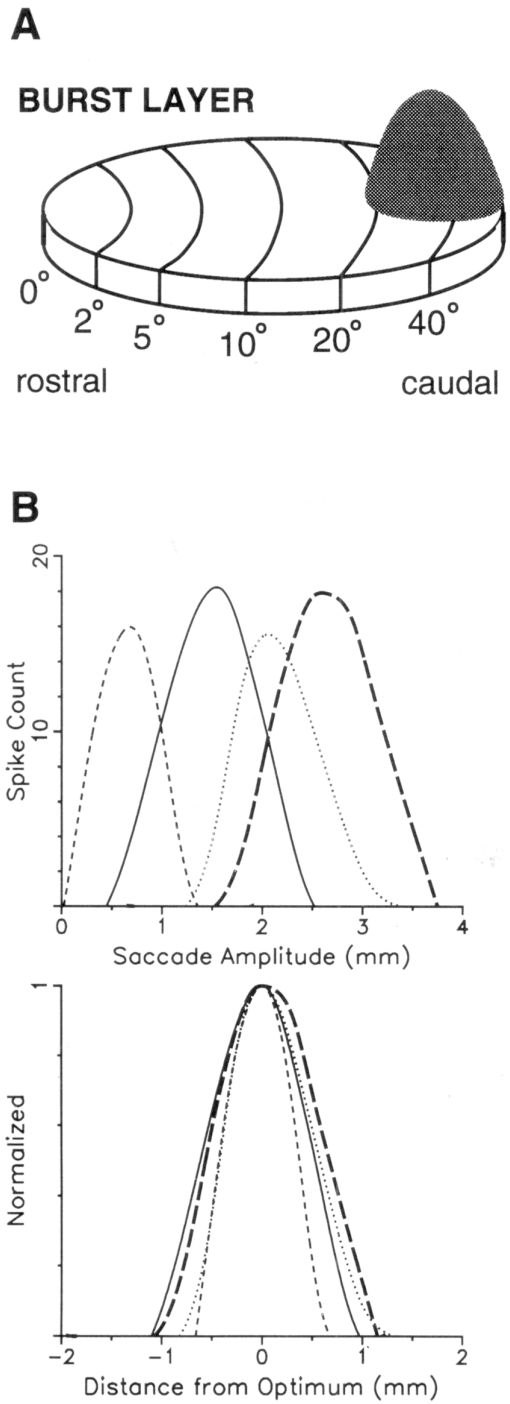

FIGURE 5. Burst cells within the superior colliculus. (**A**) Cartoon of the organization of burst cells within a layer of the superior colliculus. The visual field is represented as a two-dimensional surface extending from rostral to caudal, from the fovea (0°) to the periphery (40°). The mound in the caudal colliculus represents the population of cells that are active before a large saccade. (**B**) Size of the active zone in the burst cell layer estimated by analysis of movement fields of single burst cells. The upper graph shows spline curves through the activity of each cell for a series of saccadic amplitudes. The four representative cells all had closed movement fields. The optimal saccade amplitude for each cell was 2° (*short dashed line*), 5° (*solid line*), 9° (*dotted line*), and 16° (*long dashed line*). Saccade amplitudes have been converted from the degrees of arc measured during the experiment into millimeters along the collicular surface using an equation derived from the map shown in Figure 4B. This allows a clearer demonstration that once allowance is made for the near logarithmic compression on the collicular map, the size and shape of the movement fields in different parts of the map are similar in shape and extent. In the lower graph, the same curves have been normalized on the peak of each curve, and the curves have been superimposed to show this similarity of shape even though each curve is related to saccades of differing amplitude. In this and subsequent figures, the illustrative samples of data are taken from the references cited in the text.

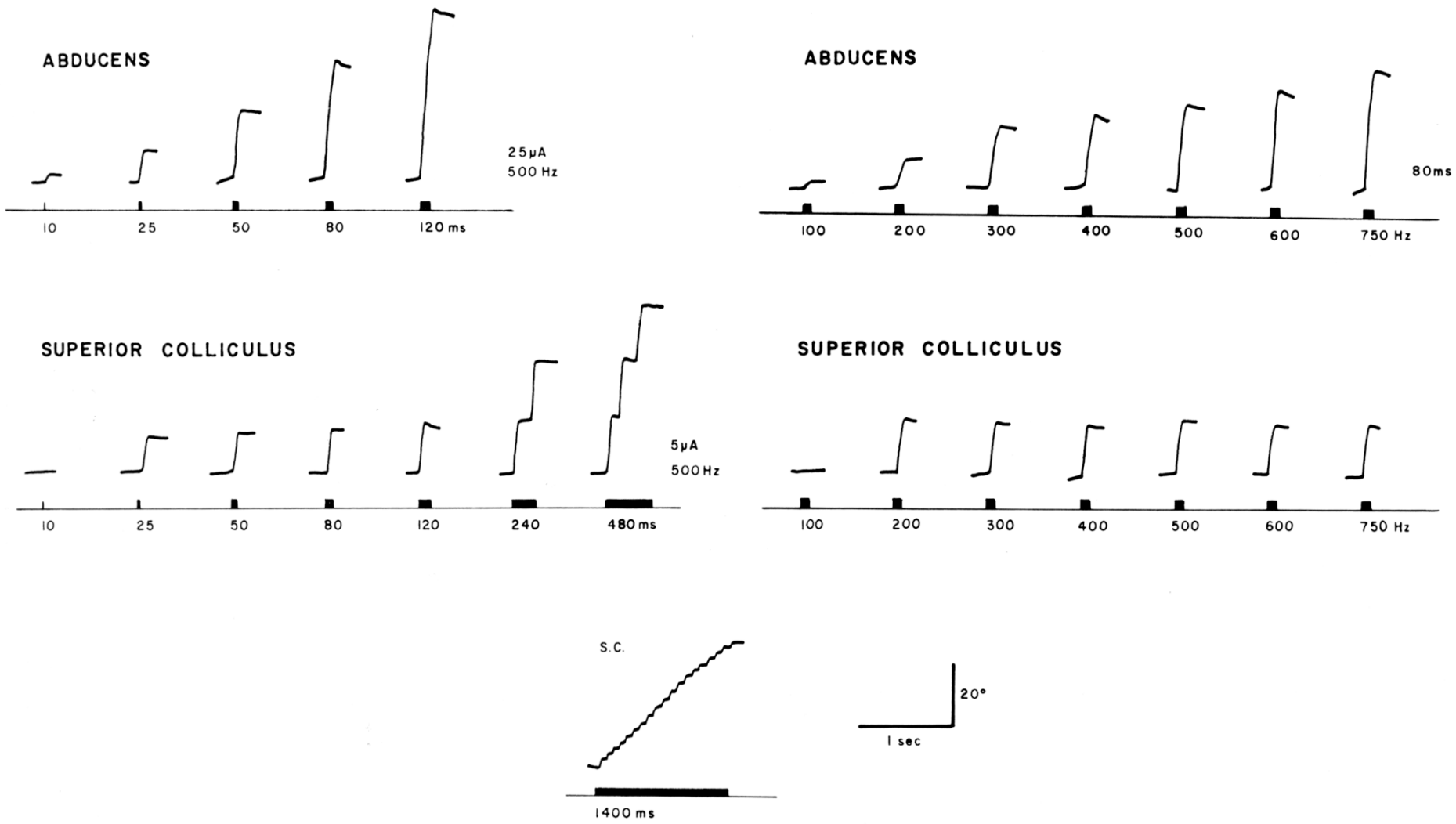

FIG. 20. Effects of electrical stimulation in abducens nucleus and superior colliculus of monkey as a function of burst duration and frequency. All eye movement records are horizontal, saccades going to the left. *Left*, stimulating frequency is constant and duration is varied; *right*, duration is constant and frequency is varied. Long staircase of saccades shown at bottom of figure was elicited by stimulating within the anterior tip of superior colliculus. [From Schiller and Stryker (206).]

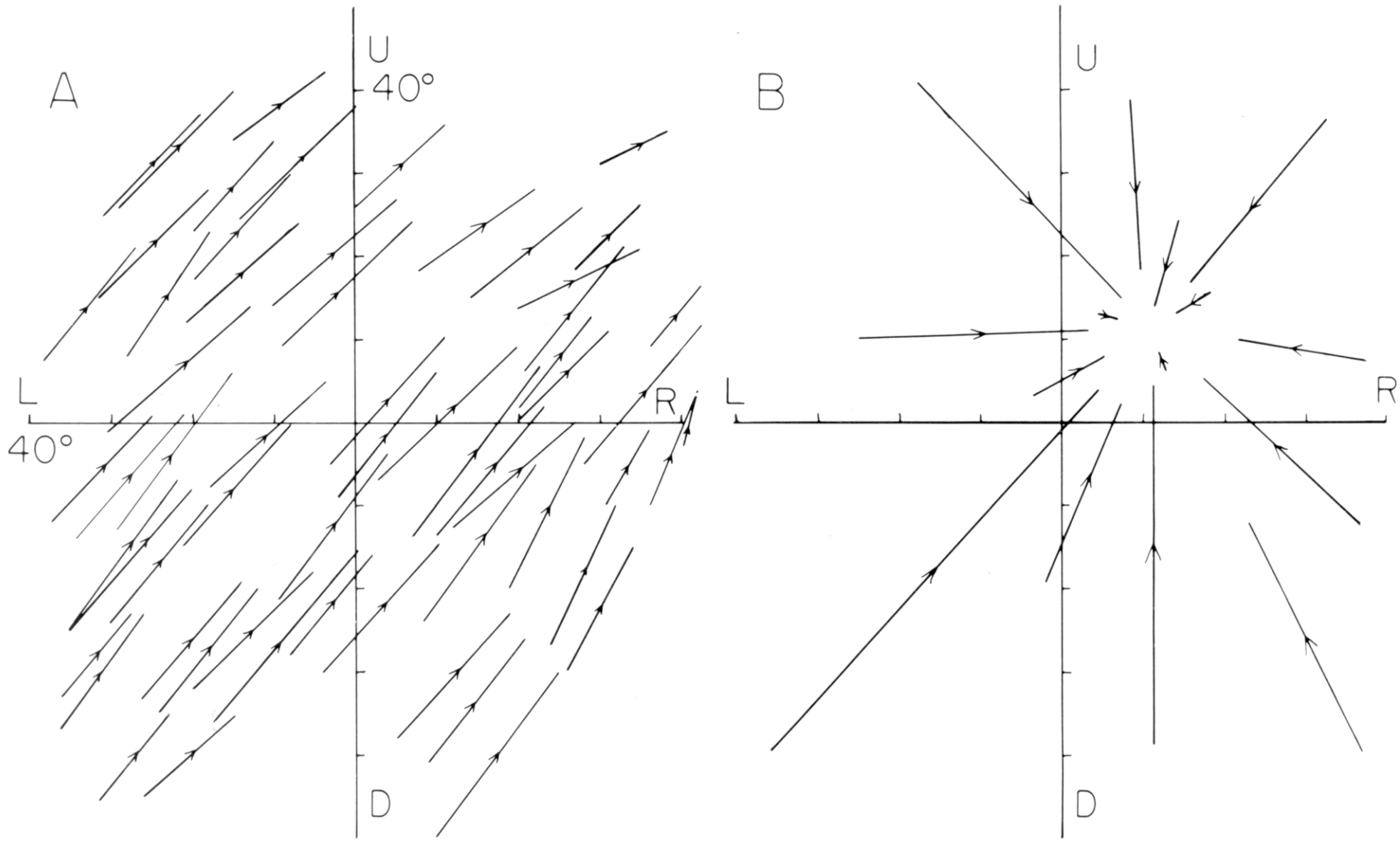

FIG. 21. Electrical stimulation of monkey colliculus: dependence of evoked saccade amplitude and direction on initial eye position. A saccade is represented as a directed line starting at initial eye position and ending at position to which saccade carried the eye. *A*: examples of colliculus-evoked saccades that did not depend on initial position. *B*: hypothetical example of way in which saccades would appear if they had been goal directed. [From Robinson (189).]

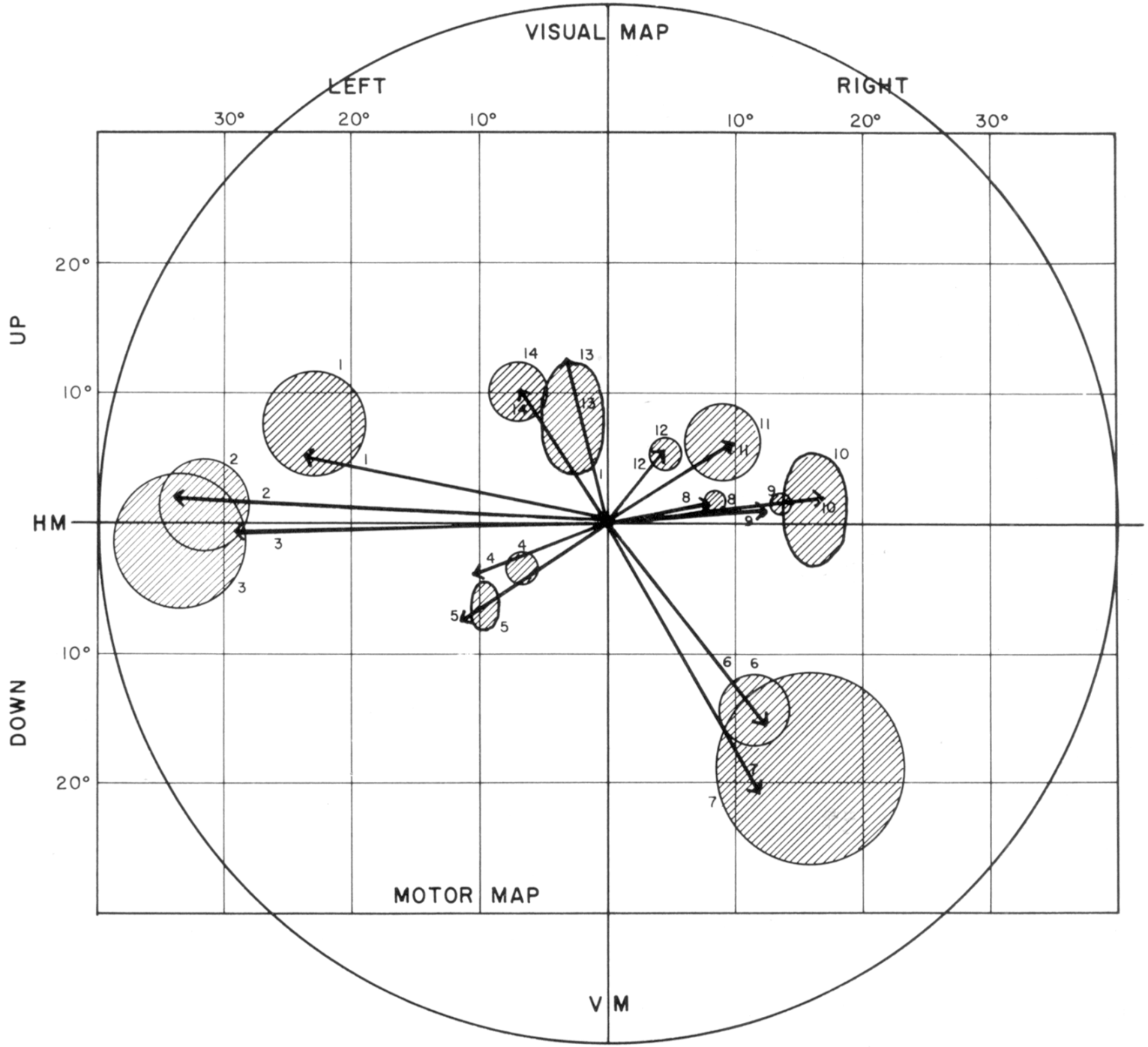
VISUAL MAP
LEFT
RIGHT
30°
20°
10°
10°
20°
30°
20°
10°
UP
HM
10°
20°
DOWN
MOTOR MAP
V M

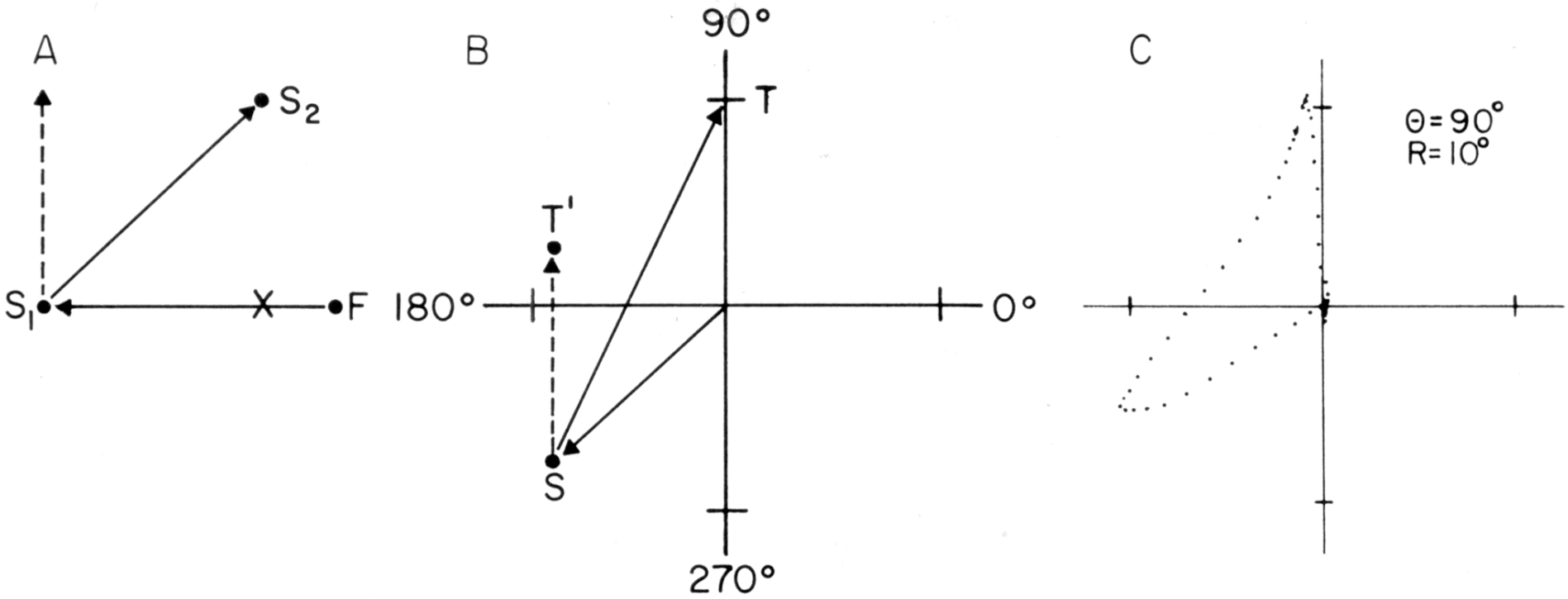

FIG. 24. Experimental procedures demonstrating that both retinal error and eye position information are used to compute size and direction of saccadic eye movements. *A*: human subject fixates in total darkness on fixation spot F, which is extinguished when stimulus S_1 is flashed. As subject initiates saccade toward S_1 (*horizontal arrow*) a second target, S_2, is flashed on at the time the eye is at position marked by ×, appearing straight up from fovea. Upon reaching position S_1 subject makes second saccade. If second saccade is straight up, only retinal error signal is computed. If second saccade is to S_2, both retinal error and eye position information are utilized. Subjects always saccade to S_2. *B*: schematic for experiment in which collicular stimulation in monkey is used to pull the eye to position S after brief appearance of target T to which animal has been trained to saccade. Utilization of retinal error signal alone should generate an eye movement to T′. Utilization of both retinal error and eye position signals should bring eye to T. *C*: two saccades are shown. For the first, going directly to T, target was flashed but colliculus was not stimulated. For the second, collicular stimulation displaced the eye toward S, but eye still ended up at T, suggesting utilization of both retinal error and eye position information. (*B*, *C*: courtesy of L. E. Mays and D. L. Sparks.)

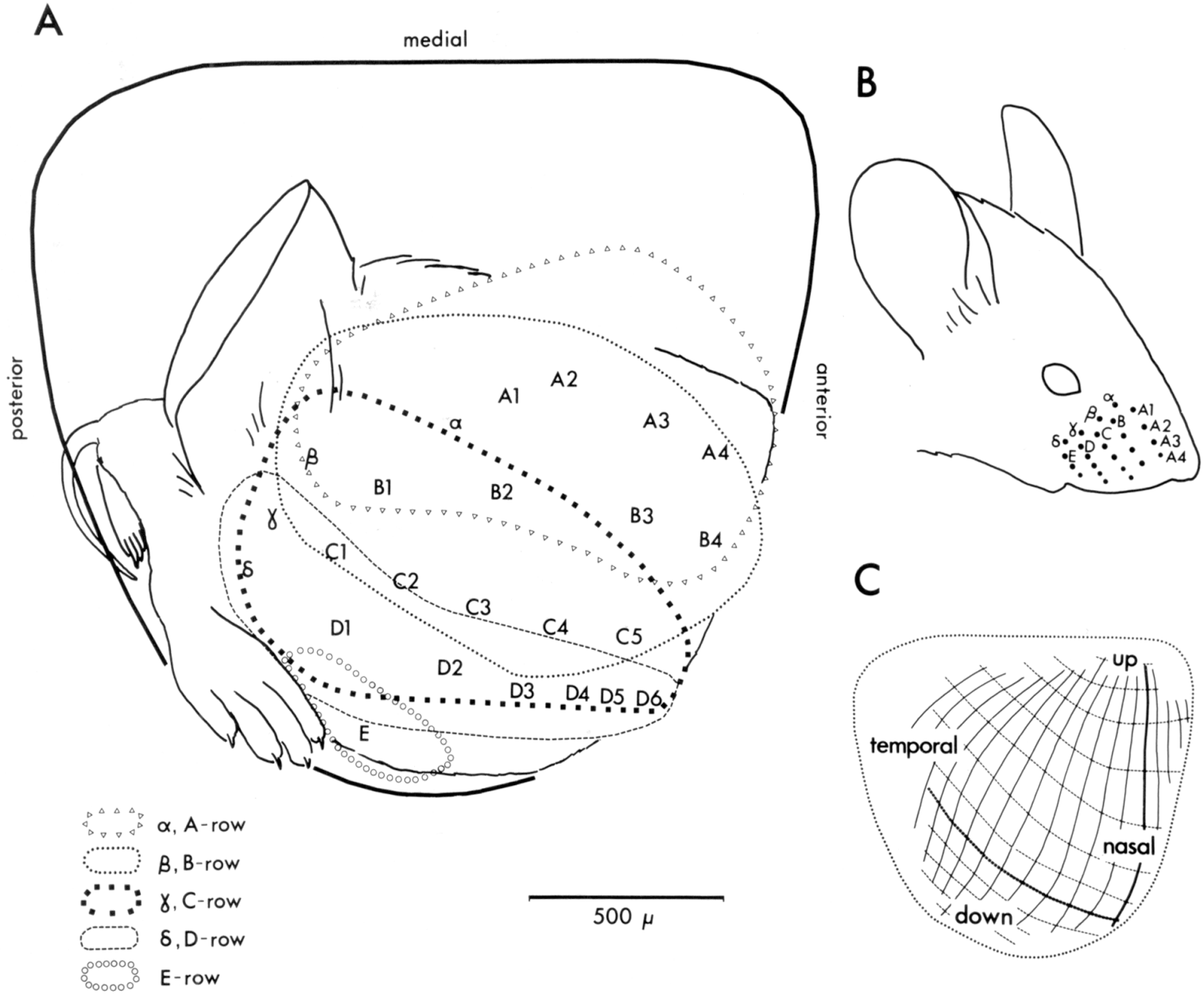

FIG. 13. *A*: map of somatosensory projection onto tectum of mouse. Letters refer to vibrissae, using notations shown in *B*; they indicate centers of tectal areas in which responses were recorded. *Ovals*, five overlapping regions within which the five rows of whiskers were represented. *B*: vibrissae. *C*: visual topography. [From Dräger and Hubel (44).]